

UNCLASSIFIED

Copy
RM E54L03

6

NACA RM E54L03



RESEARCH MEMORANDUM

INTERNAL PERFORMANCE OF A SERIES OF CIRCULAR AUXILIARY -AIR
INLETS IMMERSSED IN A TURBULENT BOUNDARY LAYER

MACH NUMBER RANGE: 1.5 to 2.0

By Paul C. Simon

Lewis Flight Propulsion Laboratory
Cleveland, Ohio

CLASSIFICATION CHANGED

UNCLASSIFIED

By authority of *Paul C. Simon*

Date *2-10-57*

CLASSIFIED DOCUMENT

UB 3-19-57

This material contains information affecting the National Defense of the United States within the meaning of the espionage laws, Title 18, U.S.C., Sec. 793 and 794, the transmission or revelation of which in any manner to an unauthorized person is prohibited by law.

NATIONAL ADVISORY COMMITTEE FOR AERONAUTICS

WASHINGTON

March 3, 1955

~~CONFIDENTIAL~~
UNCLASSIFIED

UNCLASSIFIED



NATIONAL ADVISORY COMMITTEE FOR AERONAUTICS

RESEARCH MEMORANDUMINTERNAL PERFORMANCE OF A SERIES OF CIRCULAR AUXILIARY-AIR
INLETS IMMERSSED IN A TURBULENT BOUNDARY LAYER

MACH NUMBER RANGE: 1.5 TO 2.0

By Paul C. Simon

SUMMARY

An experimental investigation was conducted to determine the internal performance characteristics of a series of circular, open-nose auxiliary air inlets immersed, by various amounts, into the supersonic, turbulent boundary layer generated by the 8- by 6-foot supersonic wind tunnel wall. Geometric variations, which were tested at nominal free-stream Mach numbers of 1.5, 1.8, and 2.0, included two inlet diameters, three lengths of inlet constant-area section, and two diffuser divergence angles.

Inlet critical total-pressure and mass-flow ratios were reasonably predicted by theory at all conditions investigated. When an inlet with a diameter approximately equal to the thickness of the approaching boundary layer was moved from the free stream at a Mach number of 1.99 to a position of complete boundary-layer immersion, the critical total-pressure recovery was reduced from 0.72 to 0.52 and the critical mass-flow ratio (referenced to free-stream conditions) dropped from unity to 0.81. During subcritical operation of this inlet, diffuser-exit static-pressure pulsations reached a maximum of approximately 11 percent of free-stream total pressure at all Mach numbers investigated.

INTRODUCTION

The need for independent auxiliary inlets to supply air to jet-exit ejectors or to accessory equipment installed on supersonic vehicles is discussed in reference 1, where the internal performance of two specific boundary-layer auxiliary inlets is reported. A more systematic investigation into the internal performance of inlets immersed in a supersonic turbulent boundary layer was indicated. Therefore, a general investigation was undertaken to determine the internal performance characteristics of a series of circular, normal-shock-type, scoop inlets immersed partly or entirely within a supersonic, turbulent boundary layer with zero pressure gradient.

UNCLASSIFIED

3535

1-00

The study was conducted in the NACA Lewis 8- by 6-foot supersonic wind tunnel at nominal free-stream Mach numbers of 1.5, 1.8, and 2.0, with the auxiliary-air inlets located in the boundary layer developed along the tunnel wall. The boundary-layer thickness was approximately equal to that predicted for the aft portion of a typical fighter fuselage. Two sharp-lip inlets were tested; one having its diameter equal to the boundary-layer thickness, and the other equal to half the boundary-layer thickness. In addition, three lengths of inlet constant-area sections and two diffuser divergence angles were evaluated. The Reynolds number per foot, based on free-stream conditions, varied between 4.44×10^6 and 5.36×10^6 .

SYMBOLS

The following symbols are used in this report:

| | |
|--------------------------|---|
| A | area |
| c_f | friction coefficient |
| D | diffuser-exit inside diameter (stations 3 and 4), in. |
| d | inlet diameter (station 1), in. |
| I/δ | inlet-boundary-layer immersion ratio (see fig. 2) |
| L | length of conical diffuser, in. |
| l | length of inlet constant-area section, in. |
| M | Mach number |
| \bar{M}_{bl}/M_0 | ratio of average Mach number at boundary-layer survey station for area equal to inlet and located at given immersion ratio to free-stream Mach number (see eq. (2)) |
| \dot{m}_{bl}/\dot{m}_0 | ratio of total mass flow, at boundary-layer survey station, through an area equal to inlet and located at given immersion ratio to mass flow through an equal area in free stream |
| P | total pressure |
| \bar{P}_{bl}/P_0 | ratio of average total pressure at boundary-layer survey station for area equal to inlet and located at given immersion ratio to free-stream total pressure (see eq. (3)) |

| | |
|---------------------------|---|
| p | static pressure |
| $(\Delta p_3/P_0)_{\max}$ | amplitude of diffuser static-pressure fluctuations, $\left(\frac{\text{max. amplitude}}{P_0}\right)$ |
| Re | Reynolds number per foot, $\rho_0 U_0 / \mu_0$ |
| T | total temperature |
| U_0 | free-stream velocity |
| u | velocity in boundary layer |
| W | weight, flow, lb/sec |
| W_c | weight-flow parameter per unit area, referenced to stan- dard sea-level conditions, $\frac{W\sqrt{T/519}}{P/2116} \frac{1}{A}$ |
| x | axial distance from station 2, in. |
| y | distance normal to tunnel wall, in. |
| β | conical-diffuser included angle, deg |
| γ | ratio of specific heats, 1.4 |
| δ | boundary-layer thickness (defined by $u/U_0 = 0.99$) at inlet station b_l , in. |
| θ | cylindrical coordinate, deg |
| μ | viscosity |
| ρ | density |
| Subscripts: | |
| b_l | plane of boundary-layer survey |
| cr | critical (highest pressure recovery in constant mass-flow range) |
| max | maximum |

- 0 free-stream conditions
 1,2,3,4 inlet stations (see fig. 4)

APPARATUS AND PROCEDURE

A series of circular, open-nose, sharp-lip, auxiliary air inlets were investigated in the 8- by 6-foot supersonic wind tunnel. The tests were conducted with the inlets mounted either on the tunnel bottom wall, with a fixed-position support system (fig. 1(a)), or on the tunnel top wall, secured by a remotely controlled boundary-layer-immersion support system (fig. 1(b)). The installations were located at a tunnel station such that the tests could be simultaneously conducted without mutual interference with another model (different test program) also mounted in the test section at the tunnel center line. The remotely controlled support system enabled the inlets to be moved, normal to the tunnel wall, from a position completely outside the tunnel boundary layer (free stream) to positions where the inlet was immersed in the boundary layer by 46, 68, and 96 percent of the boundary-layer thickness. These positions are schematically represented in figure 2.

The nine configurations investigated are illustrated in figure 3 and each is identified by three numbers: the inlet lip diameter d , the ratio of length of inlet constant-area section to inlet diameter l/d , and the conical-diffuser included angle β . Five of the models had an inlet diameter of 2 inches, which is approximately one half of the boundary-layer thickness, while the four remaining models had an inlet diameter of four inches. Three different constant-area sections behind the lip (l/d of 0.5 or 0.75, 1.5 and 3.0) and two diffuser divergence angles (6.5 and 3.5) were evaluated.

Model stations are indicated in figure 4, which depicts a typical configuration partially immersed in the boundary layer. The boundary layer generated along the tunnel wall was measured with a total-pressure rake and an adjacent static orifice, at station b_1 (immediately forward of the inlet lip station 1) without a model present. A total-pressure survey was made at inlet station 3 for the purpose of establishing the diffuser-exit total-pressure profiles. The exit area of the discharge duct was varied by longitudinal motion of a remotely controlled, mass-flow throttling plug. The mass flow and the total-pressure recovery were determined by means of static-pressure measurements at station 4 and the known sonic flow area at the duct exit assuming isentropic flow.

Dynamic-pressure pickups were connected to a tunnel-wall static-pressure orifice at station b_1 and a diffuser-wall static-pressure orifice located 2 inches upstream of station 3. The pressure fluctuations were recorded by a Brush oscillograph and were used to analyze

the amplitude of the boundary layer and inlet pressure oscillations. Tunnel boundary-layer static-pressure perturbations were found to remain constant at a negligible value of 0.2 percent of free-stream total pressure for the Mach number range from 1.5 to 2.0 with no inlet configuration present.

RESULTS AND DISCUSSION

Boundary-Layer Flow

In order to ascertain the character of the tunnel boundary layer immediately ahead of the inlet, a total-pressure survey was made on both the bottom and top tunnel walls with the inlet removed. The bottom-wall survey rake was located at a tunnel station 4 feet $5\frac{1}{2}$ inches upstream of the top-wall rake, thus resulting in a slight difference in velocity profiles. The pertinent boundary-layer information, based on free-stream conditions, such as the profile, boundary-layer thickness, Mach number outside the layer, and the Reynolds number per foot, is presented in figure 5.

The power $1/N$ of the nondimensional boundary-layer profile

$$\frac{u}{U_0} = \left(\frac{y}{\delta}\right)^{1/N}$$

was found to be $1/10$ for the bottom wall and $1/9.3$ for the top wall. These experimentally determined values, along with the established boundary-layer thickness, the free-stream Mach number, and the assumption of constant static pressure and total temperature throughout the boundary layer, were inserted in the following equation, which defines the boundary-layer mass-flow ratio that theoretically would enter a circular inlet:

$$\left(\frac{m_{bl}}{m_0}\right)_\delta = \frac{1}{A_{11}} \int \frac{M_{bl}}{M_0} \left(\frac{1 + \frac{\gamma-1}{2} M_{bl}^2}{1 + \frac{\gamma-1}{2} M_0^2} \right)^{1/2} dA \quad (1)$$

The integral was evaluated numerically. For cases where part of the inlet lip was protruding out of the boundary layer, the mass flow entering that portion was added to the values determined from equation (1), thus determining the total mass flow available to the inlet (in terms of the free-stream mass flow). The resultant mass-flow ratios are presented in figure 6 together with the mean inlet Mach number and the mean

available inlet total-pressure ratios. The mean inlet Mach number and total-pressure ratios were determined from one-dimensional continuity considerations and the evaluated total mass-flow ratio from the equations

$$\frac{\bar{M}_{bl}}{M_0} \left(\frac{1 + \frac{\gamma-1}{2} \bar{M}_{bl}^2}{1 + \frac{\gamma-1}{2} M_0^2} \right)^{1/2} = \frac{m_{bl}}{m_0} \quad (2)$$

and

$$\frac{\bar{P}_{bl}}{P_0} = \left(\frac{1 + \frac{\gamma-1}{2} \bar{M}_{bl}^2}{1 + \frac{\gamma-1}{2} M_0^2} \right)^{\frac{\gamma}{\gamma-1}} \quad (3)$$

A detailed account of methods of averaging the pertinent boundary-layer parameters, including the preceding method, may be found in references 2 and 3. Since in this report the experimental performance of the inlets investigated is presented on the basis of free-stream conditions, the characteristics based on the mean initial inlet flow conditions can be determined by utilizing the ratios of the average or mean boundary-layer to free-stream parameters presented in figure 6.

Inlet Performance

The theoretical and experimental auxiliary-inlet mass-flow and total-pressure-recovery characteristics at critical flow are summarized in table I. Complete experimental results, at nominal free-stream Mach numbers of 1.5, 1.8, and 2.0, are plotted in figure 7 for immersion ratios I/δ of zero, 0.46, 0.68, and 0.96. Lines of constant weight-flow parameter per unit area $W_{c,4}$ are presented for convenience.

With the inlets completely immersed in the boundary layer ($I/\delta = 0.96$), configuration 4-3.0-3.5 delivered the highest maximum pressure recovery, that is, 0.72 and 0.53 at Mach numbers of 1.50 and 1.99, respectively. The effect of inlet-boundary-layer immersion on the critical pressure recovery and mass-flow ratio is illustrated in figure 8(a) by the typical performance of configuration 4-3.0-3.5. As would be expected, both mass flow and pressure recovery decreased as the amount of inlet-boundary-layer immersion was increased. At a free-stream Mach number of 1.99, the critical pressure recovery was reduced from 0.72 to 0.52 and the critical mass-flow ratio dropped from unity to 0.81 when the inlet was moved from the free stream to a position of complete boundary-layer immersion.

3535

The theoretical total-pressure recoveries shown on figure 8(a) (also tabulated in table I) were determined from the normal-shock total-pressure ratio taken at the mean boundary-layer Mach number \bar{M}_{b1} , as calculated from equation (2). With the inlet immersed in the boundary layer by 96 percent, the theoretical value was calculated to be 0.55 compared with the experimental value of 0.52 at Mach number of 1.99. Even better agreement can be achieved by including the theoretical diffuser friction losses presented in reference 4, as shown in figure 8 by the solid symbols; at I/δ of 0.96 and M_0 of 1.99, the estimation of the recovery was thus improved to a value of 0.54. The inclusion of the friction losses in the theoretical prediction becomes of greater significance as the free-stream Mach number decreases. The excellent agreement between theoretical and experimental mass-flow ratios, shown in figure 8(a), indicates that the inlet captured the entire amount of air available to it (eq. (1) or fig. 6).

The effect of inlet-boundary-layer immersion on critical total-pressure recovery and mass-flow ratio, referenced to the mean boundary-layer flow condition, is presented in figure 8(b) by the performance of a typical configuration (4-3.0-3.5). The diffusion efficiency, as indicated by the changes in total-pressure recovery, improved as the inlet immersion into the boundary layer was increased. This trend might be expected, since the shock losses decrease as the average inlet Mach number is reduced and the immersion is increased. The critical mass-flow ratios and total-pressure recoveries of the rectangular, rounded-lip, boundary-layer scoop inlet of reference 1, shown on figure 9 as tailed symbols, indicate a recovery considerably lower than that of the circular inlet in addition to a mass spillage of about 25 percent (low-energy bleed-off slots were incorporated in the entrance lip of the reference inlet). The internal performance of the boundary-layer-removal scoops reported in reference 5 can also be utilized as an aid to evaluating auxiliary air supply systems.

The experimentally determined effect of inlet-boundary-layer immersion on critical weight-flow parameter $(W_{c,4})_{cr}$ is presented in figure 9(a) for configuration 2-3.0-3.5 and in figure 9(b) for configuration 4-3.0-3.5. The 2-inch-diameter inlet and the 4-inch-diameter inlet showed an increase in critical weight-flow parameter of approximately 23 percent and 13 percent, respectively, when the inlets were moved from the free stream to the wall. Such curves are convenient for studying weight-flow matching of auxiliary inlets to accessory air requirements.

The effect of changes in length of inlet constant-area section and diffuser divergence angle on inlet critical pressure recovery and mass-flow ratio is presented in figure 10(a) for the 4-inch-diameter inlet and in figure 10(b) for the 2-inch-diameter inlet at immersion ratios of zero and 0.96. The rate of change of total-pressure recovery with free-stream Mach number, for both diameter inlets and all amounts of inlet-

boundary-layer immersion, was equal to the normal-shock total-pressure-ratio relation. For complete inlet-boundary-layer immersion ($I/\delta = 0.96$) of the inlet having a diameter approximately equal to the boundary-layer thickness (fig. 10(a)) and operating at Mach number 1.99, the lengthening of the inlet constant-area section from 0.5 inlet diameter (configuration 4-0.5-6.5) to 3.0 inlet diameters (configuration 4-3.0-6.5) increased the maximum pressure recovery from 0.46 to 0.51. At the same operating conditions, a decrease in diffuser divergence angle from 6.5° (configuration 4-0.5-6.5) to 3.5° (configuration 4-0.5-3.5) increased the recovery from 0.46 to 0.50. The combined effect of the simultaneous changes in geometry from configuration 4-0.5-6.5 to 4-3.0-3.5 produced an improvement in maximum total-pressure recovery of from 0.46 to 0.53. These increases in total-pressure recovery verify the inlet design principles of mixing of nonuniform velocity profiles before diffusion and slow rate of diffusion in order to improve inlet efficiencies. Critical mass-flow ratio decreased slightly with increases in free-stream Mach number and was unaffected by the configuration geometry changes previously described.

For complete inlet-boundary-layer immersion at a free-stream Mach number of 1.99, the maximum pressure recovery of the 2-inch inlet was 0.44 (fig. 10(b)) compared with 0.53 (fig. 10(a)) for the 4-inch inlet. The lower total-pressure recovery of the 2-inch-diameter inlet is a result of capturing a smaller percentage of the high-energy air available in the upper portion of the boundary-layer profile than was captured with the larger inlet. The effect on pressure recovery of changes in length of constant-area section and diffuser angle of the 2-inch inlet was similar to that of the 4-inch inlet but reduced in magnitude.

Since good agreement was observed between the experimental data and the theoretical predictions for circular inlets, a theoretical analysis was undertaken to determine the effect of inlet frontal cross section on potential inlet performance. A sharp-lip inlet having a rectangular cross section and another having an inverted triangular cross section are compared with a circular inlet in figure 11 over a range of free-stream Mach number from 1.5 to 2.0.

All inlets were assumed to be immersed completely in a $1/7$ -power boundary-layer profile and had equal frontal areas and inlet heights equal to the boundary-layer thickness. The rectangular-inlet pressure recovery and mass-flow ratio were calculated to be slightly lower than those of the circular type; however, the performance of the triangular type showed considerable superiority over the performance of both the circular and rectangular inlets. At Mach number 2.0, the triangular shape gained 17 percent in recovery and 11 percent in mass flow over the circular shape. It is obvious from the sketch of the superimposed inlets that the inverted triangular inlet captures a greater percentage of the high-energy air existing in the upper portion of the boundary-layer profile than either the rectangular or circular inlets.

Diffuser-exit flow conditions at Mach number 1.99 are presented in figure 12 as contours of constant total-pressure ratio for various configurations and inlet-boundary-layer immersions. Figure 12(a) shows the effect of variations in inlet geometry on the exit profiles for approximately critical inlet conditions at an immersion ratio of 0.96. The contours indicate that a reduction in diffuser divergence angle from 6.5° to 3.5° caused the diffuser-exit profile to change from a symmetrical to an asymmetrical distribution (the total-pressure gradient, however, is very small). Changes in length of inlet constant-area section had little influence on the exit contours. Figure 12(b) shows an increase in the total-pressure gradient in the lower quadrant as the inlet (configuration 4-3.0-6.5) was immersed farther into the boundary layer.

Static-pressure distributions along the inlet constant-area section and subsonic diffuser are presented in figure 13 for configuration 4-3.0-3.5. The pressures were measured at a free-stream Mach number of 1.99 during subcritical, critical, and supercritical inlet operation at immersion ratios of zero and 0.96. One-dimensional estimates of the static-pressure distribution are indicated on the figure. The theoretical terminal-shock location was arbitrarily placed at the start of the experimental pressure rise. As with most duct flows, the pressure rise associated with the terminal-shock structure was distributed over several passage diameters, following which the rate of subsonic diffusion followed the predicted variation. Uniform lateral static pressure was maintained for the entire diffusion process over the mass-flow and inlet immersion range investigated.

Diffuser-Exit Pressure Fluctuations

The amplitude of the diffuser-exit static-pressure fluctuation, as determined from a dynamic-pressure pickup, is presented in figure 14 for configurations 2-3.0-3.5 and 4-3.0-3.5 at Mach numbers 1.50, 1.79, and 1.99. Negligible pressure fluctuations were recorded during operation of the inlets in the free stream; however, as the inlets were immersed in the boundary layer, the amplitude of the pressure fluctuations reached about 2 percent of free-stream total pressure in the supercritical range and increased rapidly in the subcritical range. Amplitudes as high as 11 percent of free-stream total pressure were recorded for the 4-inch-diameter inlet (fig. 14(b)), and amplitudes of about 5 percent were recorded for the 2-inch inlet (fig. 14(a)). These pressure fluctuations appear to be independent of free-stream Mach number. The amplitude of the diffuser-exit pressure fluctuations recorded during subcritical operation and complete inlet-boundary-layer immersion are of the same order of magnitude as those recorded during diffuser buzzing of the engine inlets described in reference 6. Since negligible tunnel-boundary-layer static-pressure fluctuations were measured, it can be concluded that the amplitudes recorded in the diffuser exit were probably not

associated with any initial boundary-layer pressure instability, but rather resulted from shock - boundary-layer interaction or adverse effects of nonuniform velocity profiles entering the diffuser, or both.

SUMMARY OF RESULTS

An experimental investigation was conducted to determine the internal performance characteristics of a series of circular, open-nose inlets immersed in the boundary layer generated by the 8- by 6-foot supersonic wind tunnel wall. A summary of the more important findings is as follows:

1. Critical total-pressure recovery and mass flow of a circular, open-nose, sharp-lip, auxiliary inlet immersed in a two-dimensional, supersonic, turbulent boundary layer can be reasonably predicted by theory.
2. At a free-stream Mach number of 1.99, the critical total-pressure recovery of the inlet with a diameter approximately equal to the thickness of the approaching boundary layer was reduced from 0.72 to 0.52 and the critical mass-flow ratio dropped from unity to 0.81 when the inlet was moved from the free stream to a position of complete boundary-layer immersion.
3. For the inlet with a diameter equal to the tunnel boundary-layer thickness and completely immersed in the boundary layer at a free-stream Mach number of 1.99, the maximum total-pressure recovery was increased from 0.46 to 0.53 by simultaneously lengthening the inlet constant-area section from 0.5 to 3.0 inlet diameters and decreasing the diffuser divergence angle from 6.5° to 3.5° .
4. For complete inlet-boundary-layer immersion at a free-stream Mach number of 1.99, the maximum pressure recovery of the inlet with a diameter approximately equal to one-half the boundary-layer thickness was 0.44, compared with 0.53 for the inlet with a diameter approximately equal to the boundary-layer thickness.
5. The series of inlets tested captured the entire amount of air available to them during critical operation at all percentages of inlet-boundary-layer immersion.
6. Amplitudes of the diffuser-exit static-pressure fluctuations reached a maximum of 11 percent of free-stream total pressure during subcritical operation of the 4-inch-diameter inlet immersed completely in the tunnel boundary layer. Pressure amplitudes of the 4-inch-diameter inlets were twice those of the 2-inch-diameter inlets in the Mach number range investigated. The diffuser-exit static pressure remained steady

during free-stream operation of all inlets throughout the mass-flow range.

Lewis Flight Propulsion Laboratory
National Advisory Committee for Aeronautics
Cleveland, Ohio, December 13, 1954

REFERENCES

1. Pennington, Donald B., and Simon, Paul C.: Internal Performance at Mach Numbers to 2.0 of Two Auxiliary Inlets Immersed in Fuselage Boundary Layer. NACA RM E53L28b, 1954.
2. Wyatt, DeMarquis D.: Analysis of Errors Introduced by Several Methods of Weighting Nonuniform Duct Flows. NACA TN 3400.
3. McLafferty, George: Theoretical Pressure Recovery Through a Normal Shock in a Duct with Initial Boundary Layer. Jour. Aero. Sci., vol. 20, no. 3, Mar. 1953, pp. 169-174.
4. Beeton, A. B. P.: Curves for the Theoretical Skin Friction Loss in Air Intake Ducts. Tech. Note AERO. 2035, British R.A.E., Feb. 1950.
5. Piercy, Thomas G., and Johnson, Harry W.: A Comparison of Several Systems of Boundary-Layer Removal Ahead of a Typical Conical External-Compression Side Inlet at Mach Numbers of 1.88 and 2.93. NACA RM E53F16, 1953.
6. Simon, Paul C.: Performance Characteristics at Mach Numbers to 2.0 of Various Types of Side Inlets Mounted on Fuselage of Proposed Supersonic Airplane. IV - Rectangular-Cowl Inlets with Two-Dimensional Compression Ramps. NACA RM E52H29, 1952.

3535

CG-2, back

TABLE I. - SUMMARY OF EXPERIMENTAL AND THEORETICAL CRITICAL INLET PRESSURE-RECOVERY AND MASS-FLOW RATIOS

12

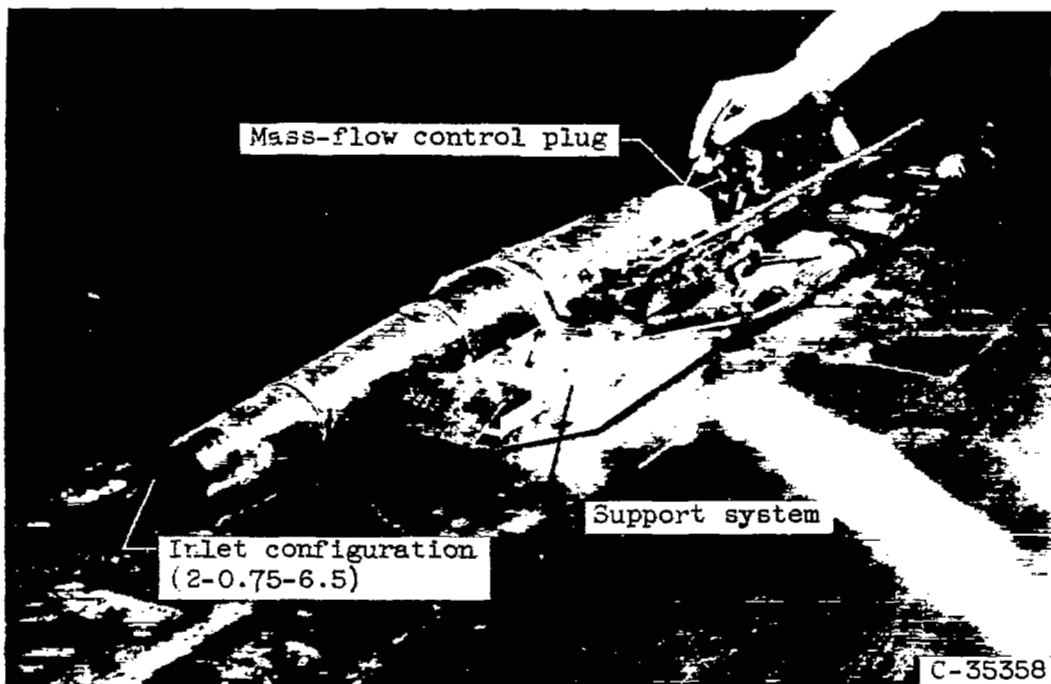
| Configuration, $d - \frac{l}{d} - \beta$ | Nominal free- stream Mach number, M_0 | Immersion ratio, l/δ | | | | | | | | | | | | | | | |
|---|--|-----------------------------|-------------------|-------------------|-------------------|-------------------|-------------------|-------------------|-------------------|-------------------|-------------------|-------------------|-------------------|-------------------|-------------------|-------------------|-------------------|
| | | 0 | | | | 0.48 | | | | 0.68 | | | | 0.96 | | | |
| | | Experiment | | Theory | | Experiment | | Theory | | Experiment | | Theory | | Experiment | | Theory | |
| | | $\frac{P_4}{P_0}$ | $\frac{m_4}{m_0}$ | $\frac{P_4}{P_0}$ | $\frac{m_4}{m_0}$ | $\frac{P_4}{P_0}$ | $\frac{m_4}{m_0}$ | $\frac{P_4}{P_0}$ | $\frac{m_4}{m_0}$ | $\frac{P_4}{P_0}$ | $\frac{m_4}{m_0}$ | $\frac{P_4}{P_0}$ | $\frac{m_4}{m_0}$ | $\frac{P_4}{P_0}$ | $\frac{m_4}{m_0}$ | $\frac{P_4}{P_0}$ | $\frac{m_4}{m_0}$ |
| 2-0.75-6.5 | 1.5 | 0.92 | 1.0 | 0.93 | 1.0 | ^b 0.85 | ^b 0.98 | ^b 0.83 | ^b 0.91 | ^b 0.78 | ^b 0.93 | ^b 0.81 | ^b 0.90 | 0.61 | ^c | 0.63 | 0.75 |
| | 1.8 | .81 | 1.0 | .82 | 1.0 | ^b 0.77 | ^b 0.98 | ^b 0.72 | ^b 0.90 | ^b 0.66 | ^b 0.92 | ^b 0.70 | ^b 0.88 | .50 | ^c | .57 | .73 |
| | 2.0 | .72 | 1.0 | .73 | 1.0 | ^b 0.67 | ^b 0.98 | ^b 0.63 | ^b 0.90 | ^b 0.58 | ^b 0.91 | ^b 0.61 | ^b 0.87 | .42 | 0.71 | .46 | .70 |
| 2-1.5-6.5 | 1.5 | ---- | ---- | 0.93 | 1.0 | ---- | ---- | ^b 0.83 | ^b 0.91 | ^b 0.77 | ^b 0.96 | ^b 0.81 | ^b 0.90 | ---- | ---- | 0.63 | 0.76 |
| | 1.8 | ---- | ---- | .82 | 1.0 | ---- | ---- | ^b 0.72 | ^b 0.90 | ^b 0.67 | ^b 0.93 | ^b 0.70 | ^b 0.88 | ---- | ---- | .57 | .73 |
| | 2.0 | ---- | ---- | .73 | 1.0 | ---- | ---- | ^b 0.63 | ^b 0.90 | ^b 0.59 | ^b 0.93 | ^b 0.61 | ^b 0.87 | ---- | ---- | .46 | .70 |
| 2-3.0-6.5 | 1.5 | 0.90 | 1.0 | 0.85 | 1.0 | ^b 0.84 | ^b 0.98 | ^b 0.83 | ^b 0.91 | ^b 0.75 | ^b 0.94 | ^b 0.81 | ^b 0.90 | 0.63 | ^c | 0.63 | 0.76 |
| | 1.8 | .80 | 1.0 | .82 | 1.0 | ^b 0.77 | ^b 0.98 | ^b 0.72 | ^b 0.90 | ^b 0.68 | ^b 0.92 | ^b 0.70 | ^b 0.88 | .51 | ^c | .57 | .73 |
| | 2.0 | .71 | 1.0 | .73 | 1.0 | ^b 0.67 | ^b 0.98 | ^b 0.63 | ^b 0.90 | ^b 0.59 | ^b 0.92 | ^b 0.61 | ^b 0.87 | .43 | ^c | .46 | .70 |
| 2-0.75-3.5 | 1.5 | ^b 0.81 | ^b 1.0 | ^b 0.93 | ^b 1.0 | ^b 0.87 | ^b 0.98 | ^b 0.83 | ^b 0.91 | ^b 0.78 | ^b 0.95 | ^b 0.81 | ^b 0.90 | 0.62 | ^c | 0.63 | 0.76 |
| | 1.8 | ^b 0.81 | ^b 1.0 | ^b 0.82 | ^b 1.0 | ^b 0.77 | ^b 0.97 | ^b 0.72 | ^b 0.90 | ^b 0.70 | ^b 0.93 | ^b 0.70 | ^b 0.88 | .51 | 0.73 | .57 | .73 |
| | 2.0 | ^b 0.72 | ^b 1.0 | ^b 0.72 | ^b 1.0 | ^b 0.68 | ^b 0.97 | ^b 0.63 | ^b 0.90 | ^b 0.61 | ^b 0.92 | ^b 0.61 | ^b 0.87 | .42 | .71 | .46 | .70 |
| 2-3.0-3.5 | 1.5 | ---- | ---- | 0.95 | 1.0 | ---- | ---- | 0.85 | 0.94 | 0.72 | 0.89 | 0.78 | 0.88 | 0.63 | ^c | 0.83 | 0.78 |
| | 1.8 | 0.80 | 1.0 | .82 | 1.0 | 0.74 | 0.85 | .75 | .93 | .85 | .88 | .68 | .86 | .52 | ^c | .97 | .73 |
| | 2.0 | .70 | 1.0 | .73 | 1.0 | ---- | ---- | .65 | .92 | .56 | .86 | .58 | .84 | .44 | ^c | .46 | .70 |
| 4-0.5-6.5 | 1.5 | 0.82 | 1.0 | 0.85 | 1.0 | 0.86 | 0.97 | 0.90 | 0.97 | 0.79 | 0.95 | 0.85 | 0.93 | 0.67 | ^c | 0.74 | 0.85 |
| | 1.8 | ---- | ---- | .82 | 1.0 | ---- | ---- | .79 | .97 | ---- | ---- | .75 | .93 | .58 | 0.83 | .65 | .83 |
| | 2.0 | .72 | 1.0 | .73 | 1.0 | .68 | .97 | .70 | .97 | .60 | .92 | .64 | .91 | .48 | ^a | .55 | .81 |
| 4-3.0-6.5 | 1.5 | 0.80 | 1.0 | 0.85 | 1.0 | 0.85 | 0.98 | 0.90 | 0.97 | 0.79 | 0.96 | 0.85 | 0.93 | 0.71 | ^c | 0.74 | 0.85 |
| | 1.8 | .81 | 1.0 | .82 | 1.0 | .75 | .99 | .79 | .97 | .70 | .94 | .75 | .93 | .59 | 0.83 | .65 | .83 |
| | 2.0 | .71 | 1.0 | .73 | 1.0 | .67 | .98 | .70 | .97 | .61 | .92 | .64 | .91 | .51 | .82 | .55 | .81 |
| 4-0.5-3.5 | 1.5 | 0.82 | 1.0 | 0.93 | 1.0 | ---- | ---- | 0.90 | 0.97 | 0.83 | 0.96 | 0.85 | 0.93 | 0.70 | ^c | 0.74 | 0.85 |
| | 1.8 | .82 | 1.0 | .82 | 1.0 | ---- | ---- | .79 | .97 | .70 | .94 | .75 | .93 | .58 | 0.84 | .65 | .83 |
| | 2.0 | .72 | 1.0 | .73 | 1.0 | ---- | ---- | .70 | .97 | .62 | .93 | .64 | .91 | .50 | .81 | .55 | .81 |
| 4-3.0-3.5 | 1.5 | 0.90 | 1.0 | 0.93 | 1.0 | 0.87 | 0.98 | 0.90 | 0.97 | 0.80 | 0.96 | 0.85 | 0.93 | 0.72 | ^c | 0.74 | 0.85 |
| | 1.8 | .79 | 1.0 | .82 | 1.0 | .77 | .88 | .79 | .97 | .72 | .93 | .75 | .93 | .61 | 0.83 | .65 | .83 |
| | 2.0 | .72 | 1.0 | .73 | 1.0 | .69 | .86 | .70 | .97 | .62 | .92 | .64 | .91 | .53 | .81 | .55 | .81 |

^aMaximum subcritical.

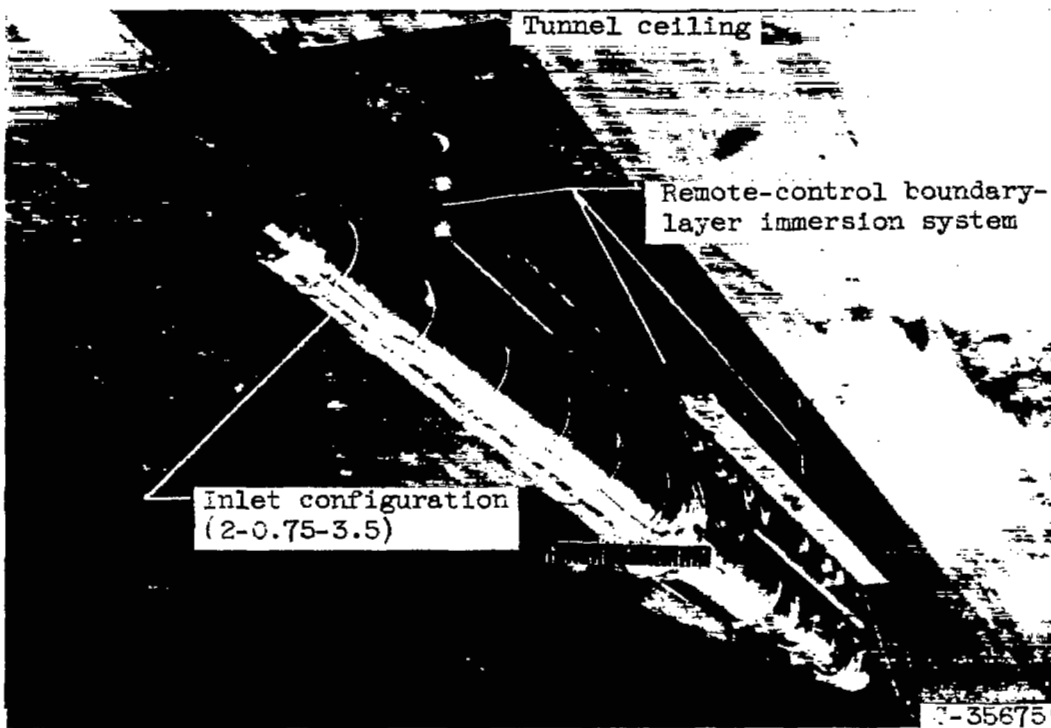
^bBottom-wall installation.

^cIndeterminable.

NACA RM ES4103

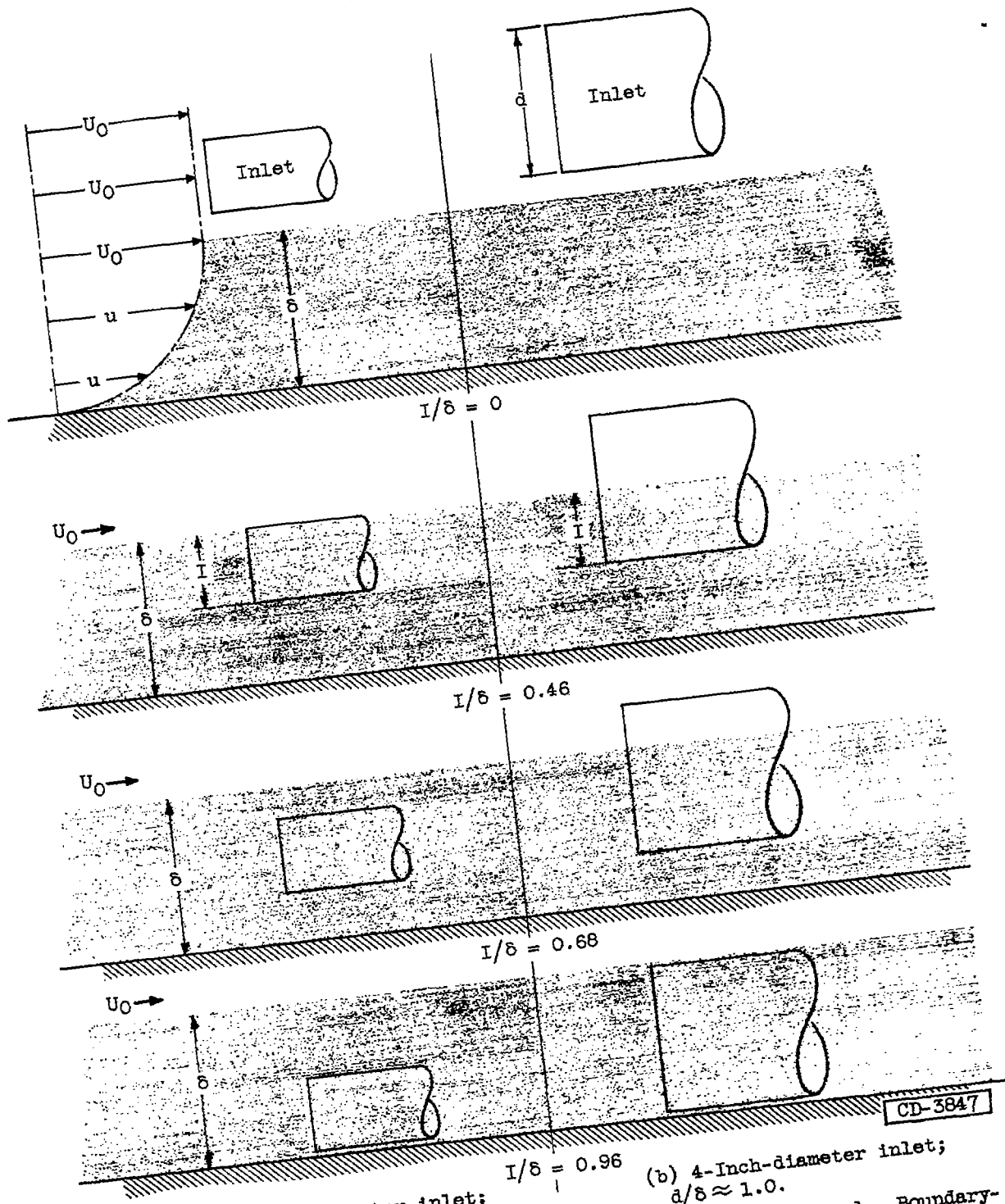


(a) Bottom wall installation (fixed position).



(b) Top wall installation (remotely controlled boundary-layer immersion).

Figure 1. - Models installed in 8- by 6-foot supersonic wind tunnel.



(a) 2-Inch-diameter inlet;
 $d/\delta \approx 0.5$.
 (b) 4-Inch-diameter inlet;
 $d/\delta \approx 1.0$.
 Figure 2. - Inlet-boundary-layer immersion ratios investigated. Boundary-layer thickness, δ , approximately 4 inches.

CD-3847

| Configuration, d-l/d-β | Dimensions | | | | |
|---------------------------|------------|------|------|-------|--------|
| | d | D | l | L | β, deg |
| 2-0.75-6.5 | 2.0 | 3.78 | 1.5 | 15.70 | 6.5 |
| 2-1.5-6.5 | 2.0 | 3.78 | 3.0 | 15.70 | 6.5 |
| 2-3.0-6.5 | 2.0 | 3.78 | 6.0 | 15.70 | 6.5 |
| 2-0.75-3.5 | 2.0 | 3.78 | 1.5 | 29.20 | 3.5 |
| 2-3.0-3.5 | 2.0 | 3.78 | 6.0 | 29.20 | 3.5 |
| 4-0.5-6.5 | 4.0 | 7.56 | 2.0 | 31.41 | 6.5 |
| 4-3.0-6.5 | 4.0 | 7.56 | 12.0 | 31.41 | 6.5 |
| 4-0.5-3.5 | 4.0 | 7.56 | 2.0 | 58.41 | 3.5 |
| 4-3.0-3.5 | 4.0 | 7.56 | 12.0 | 58.41 | 3.5 |

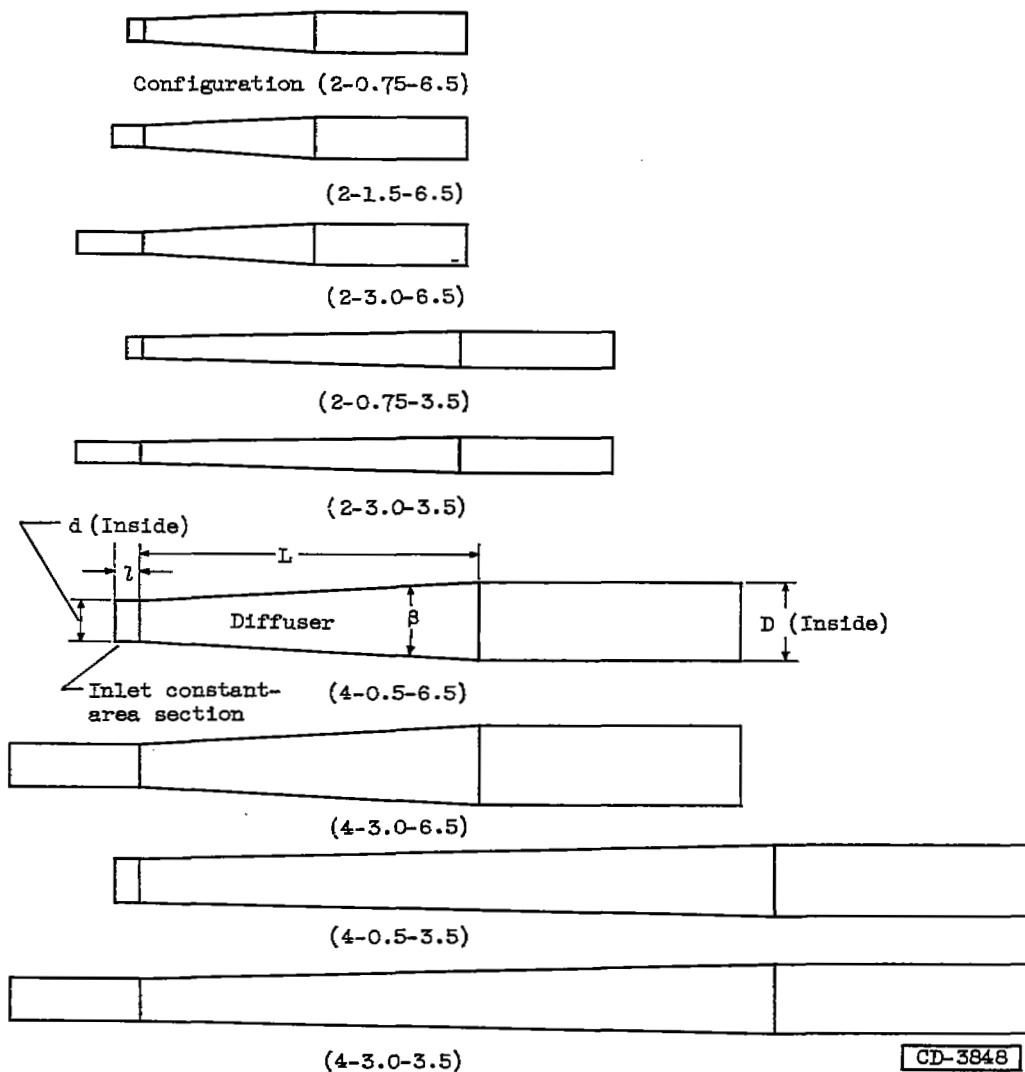


Figure 3. - Test model configurations (all dimensions in inches).

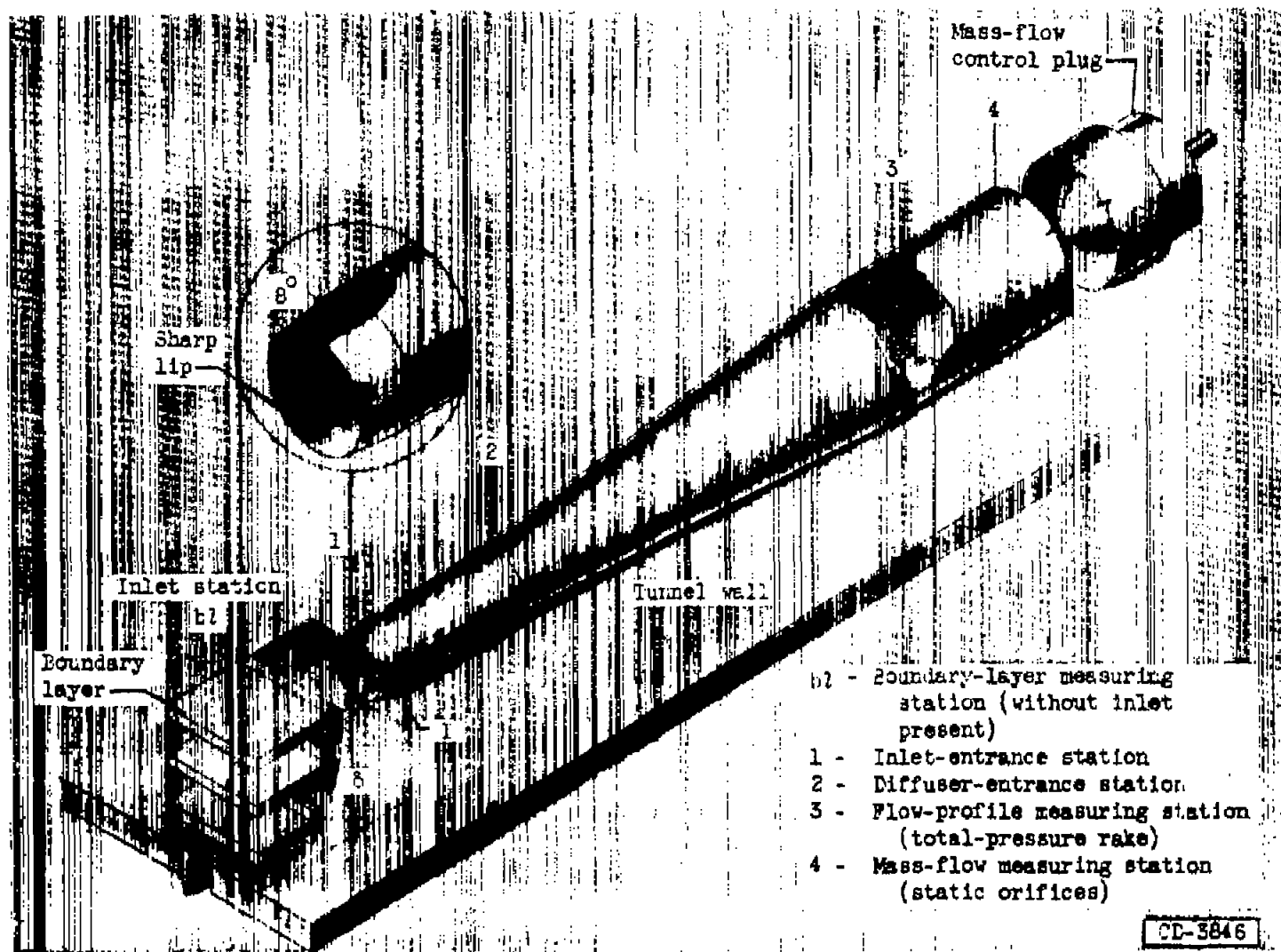
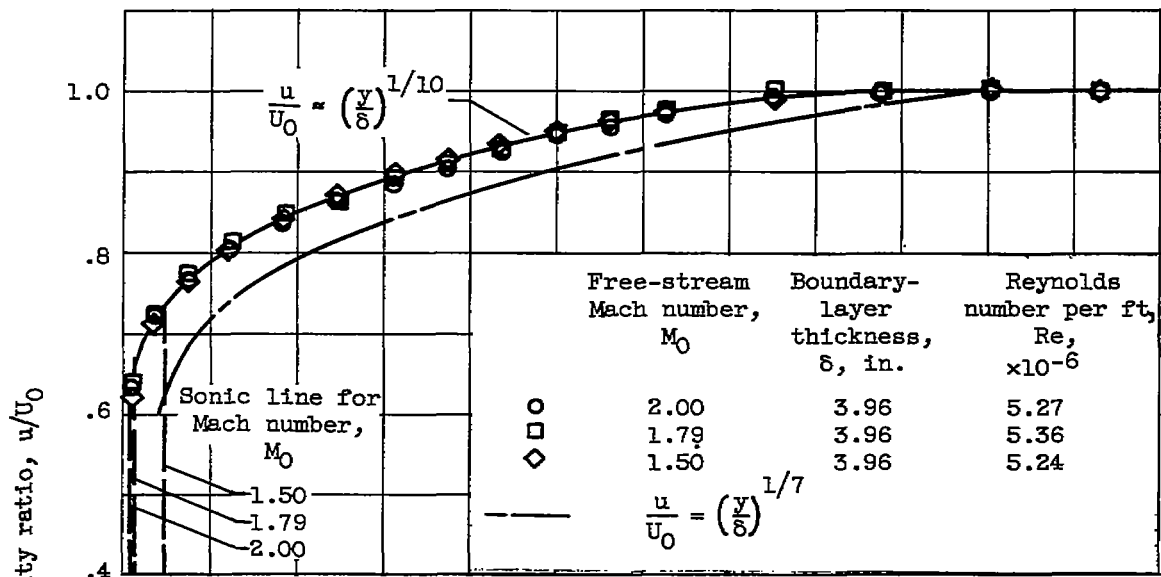
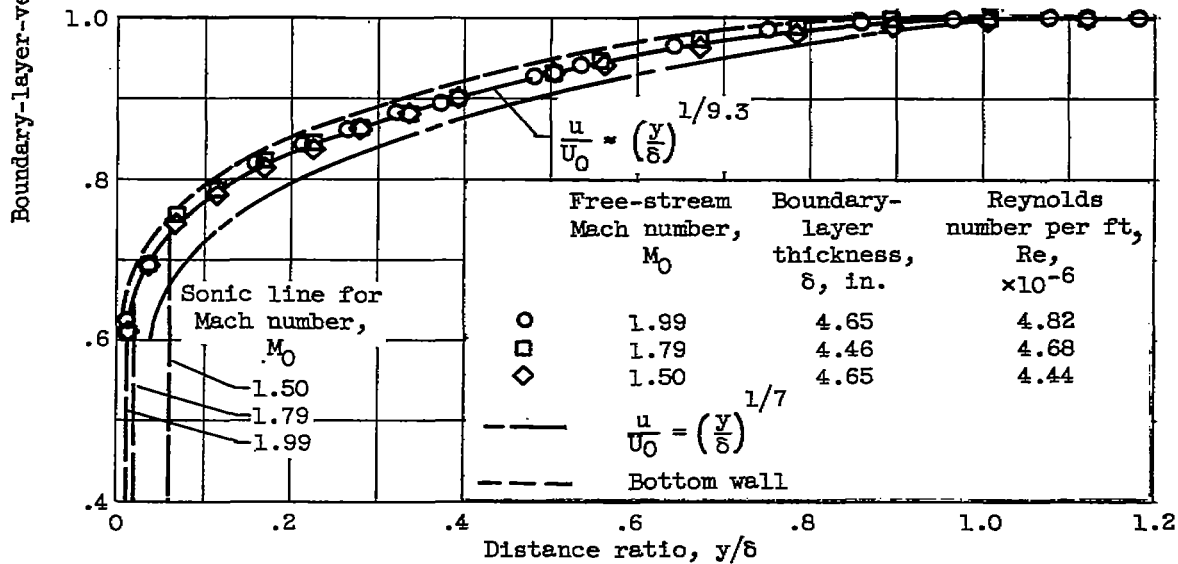


Figure 4. - Isometric view of typical model. Ratio of diffuser-exit area to inlet area, A_4/A_1 , 3.570.



(a) Bottom wall.



(b) Top wall.

Figure 5. - Boundary-layer profiles ahead of inlets (inlet not present).

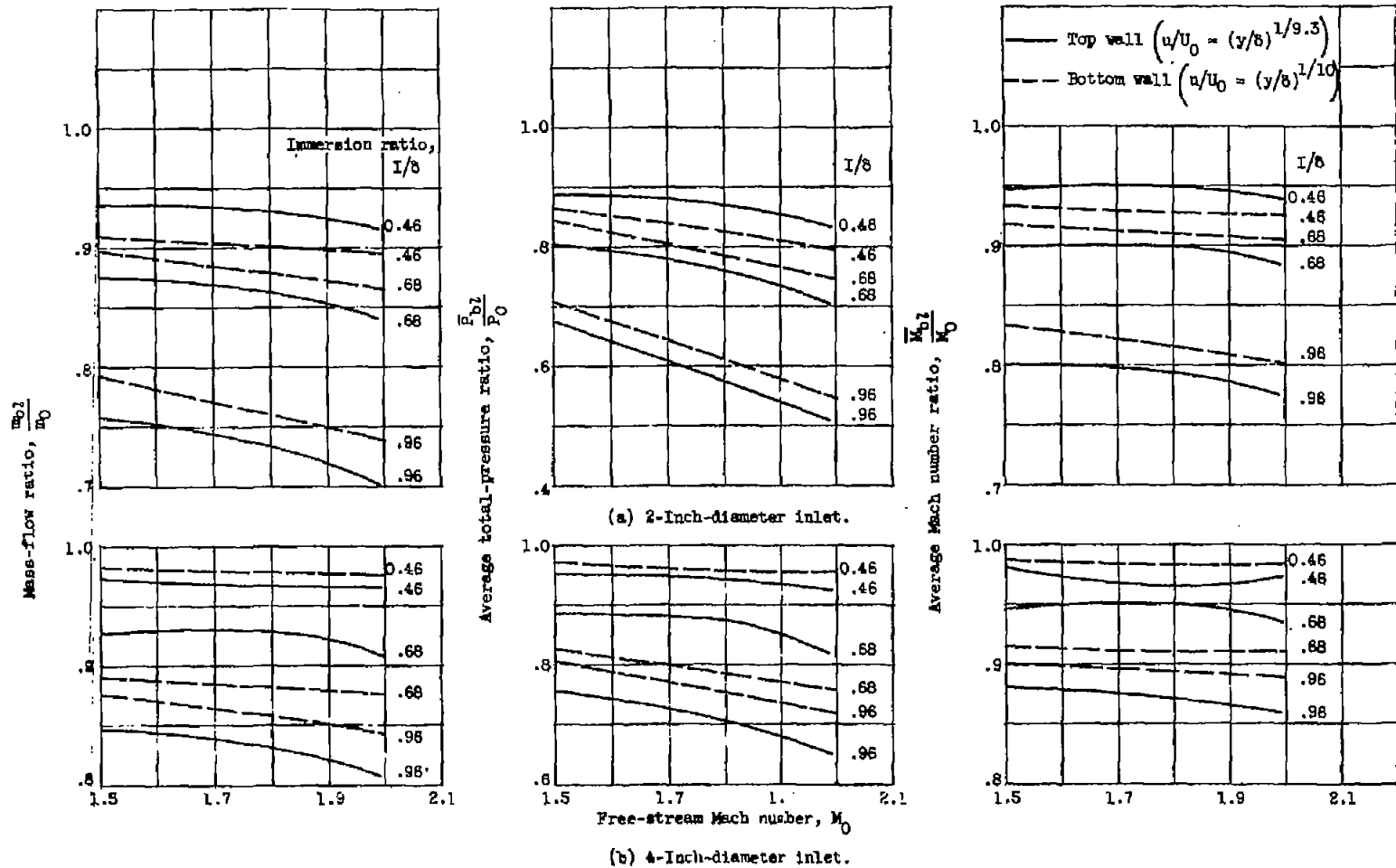


Figure 6. - Boundary-layer flow parameters averaged across inlet area and referred to free-stream flow conditions.

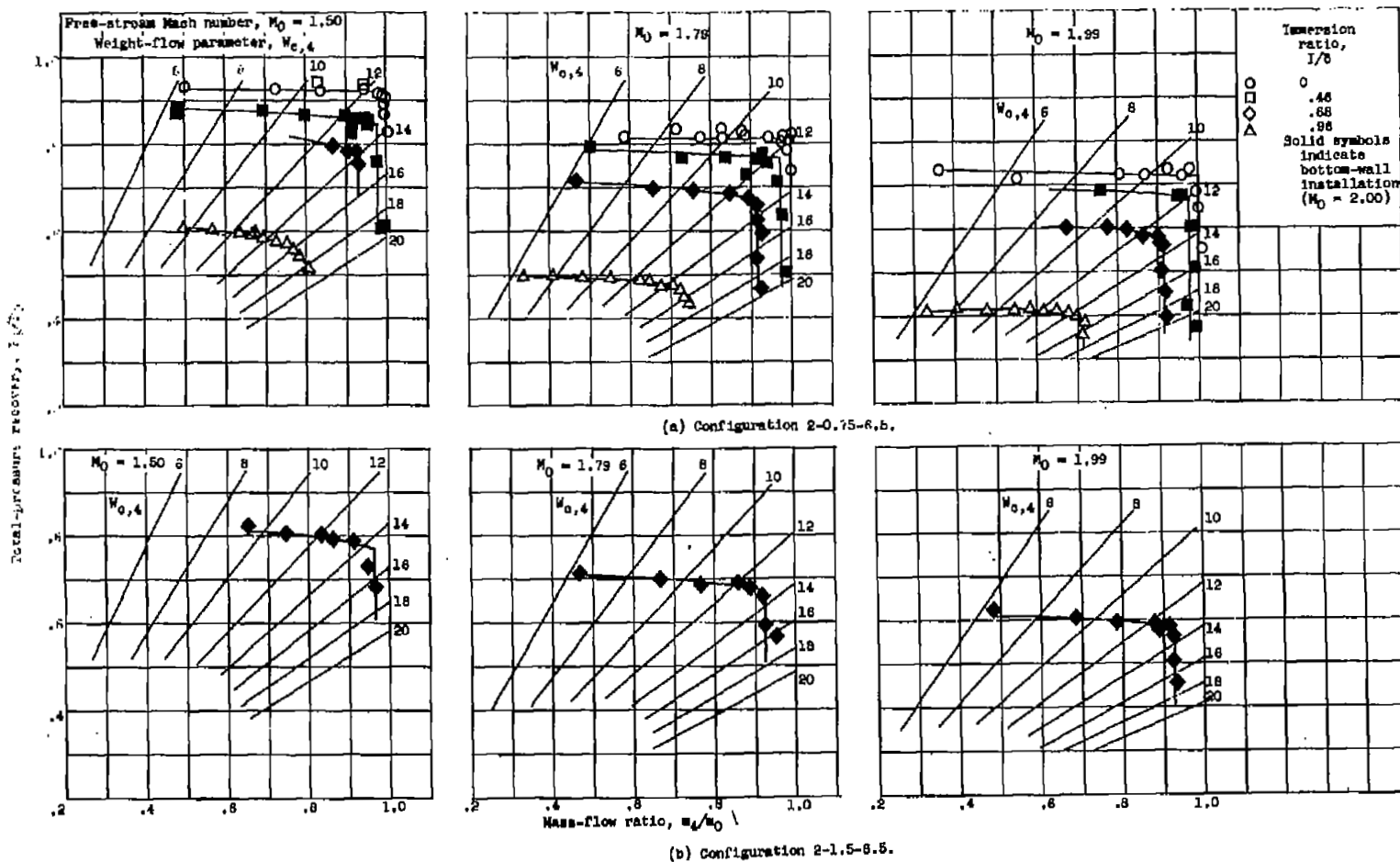


Figure 7. - Inlet total-pressure recovery.

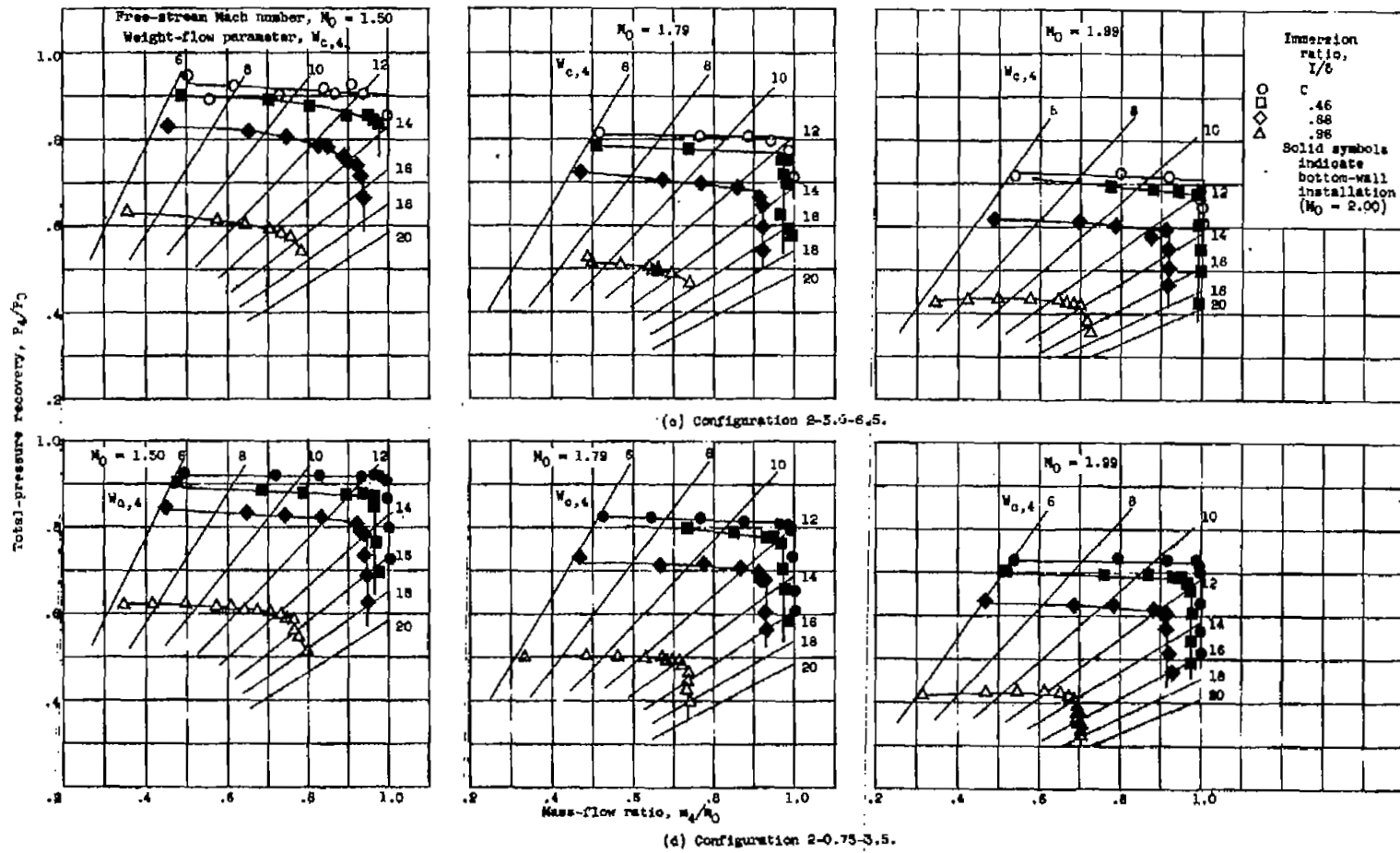


Figure 7. - Continued. Inlet total-pressure recovery.

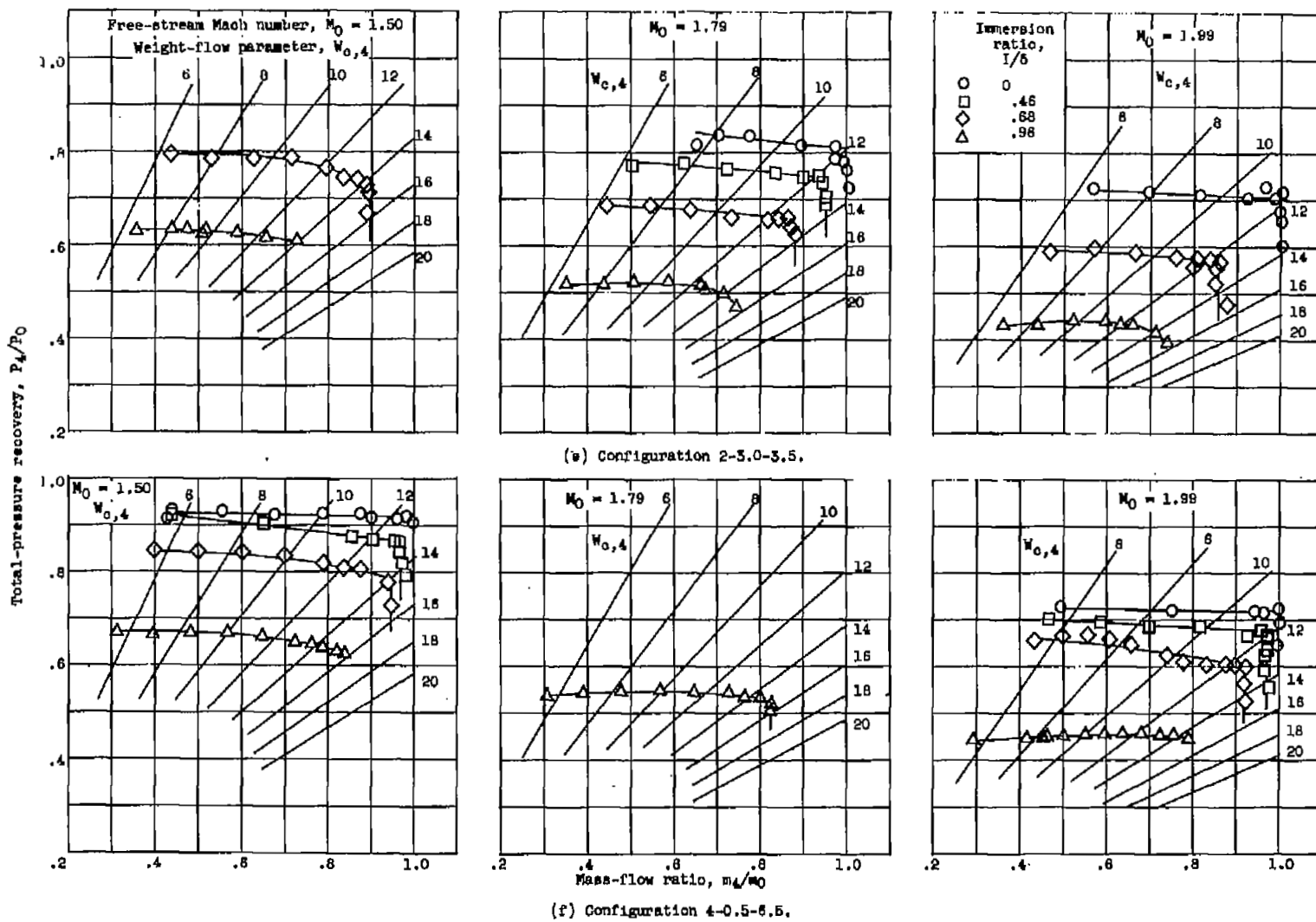


Figure 7. - Continued. Inlet total-pressure recovery.

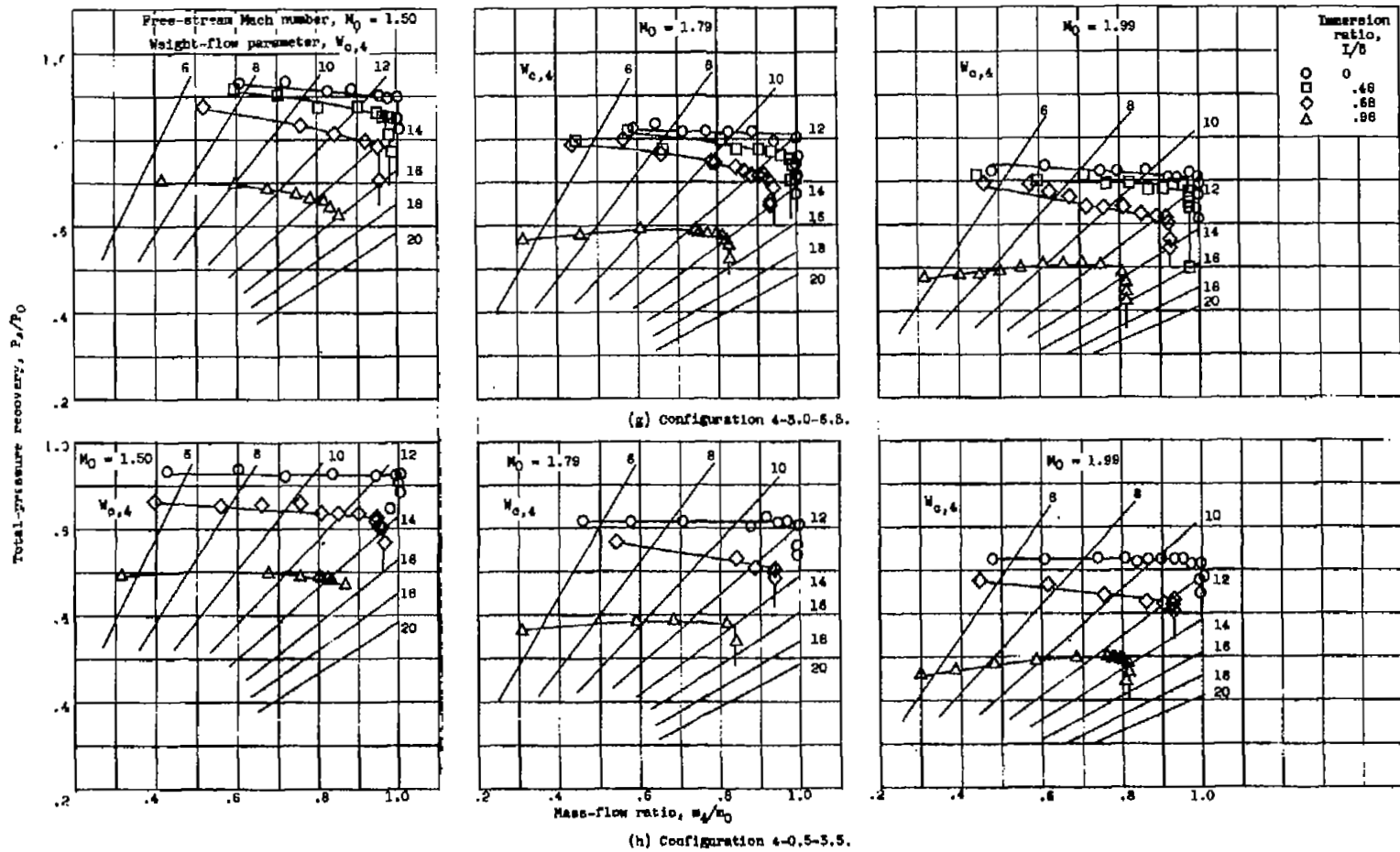
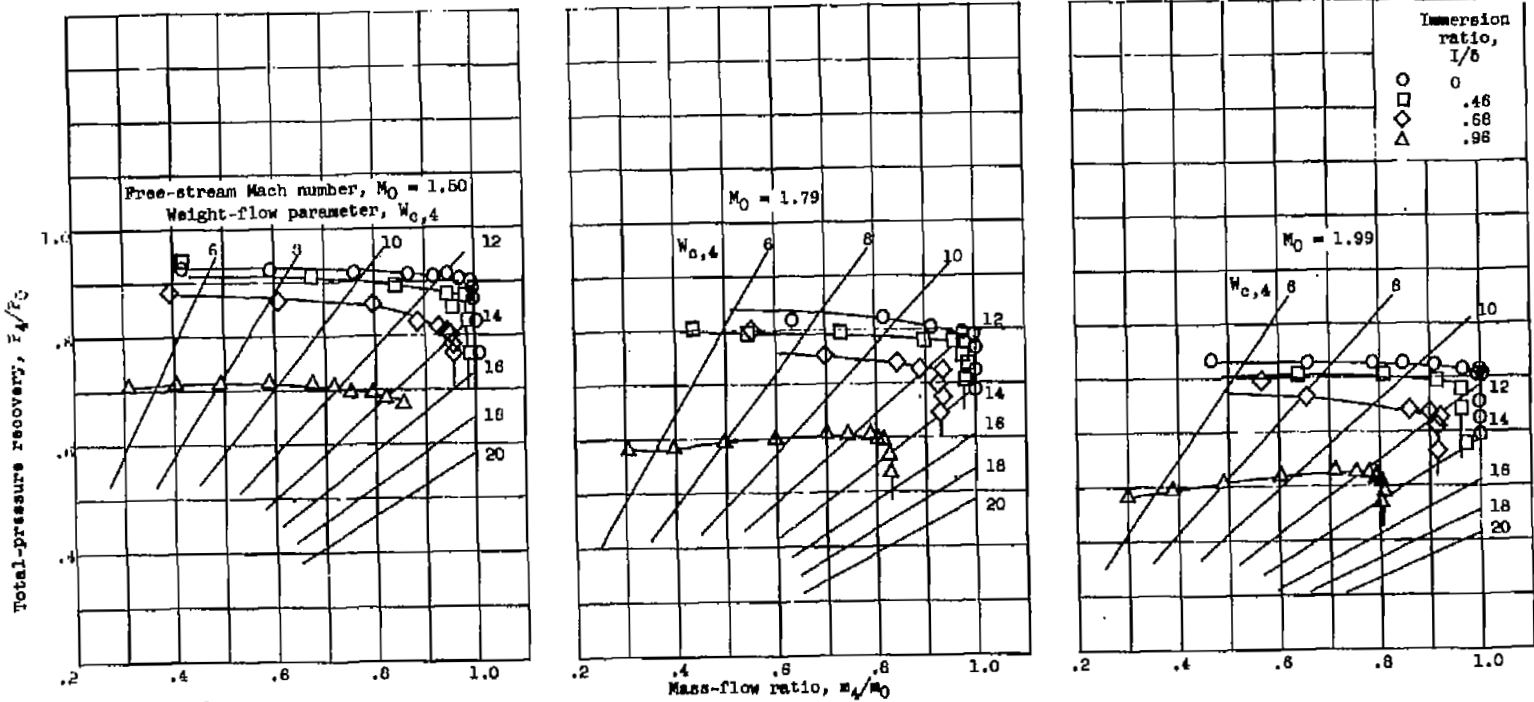
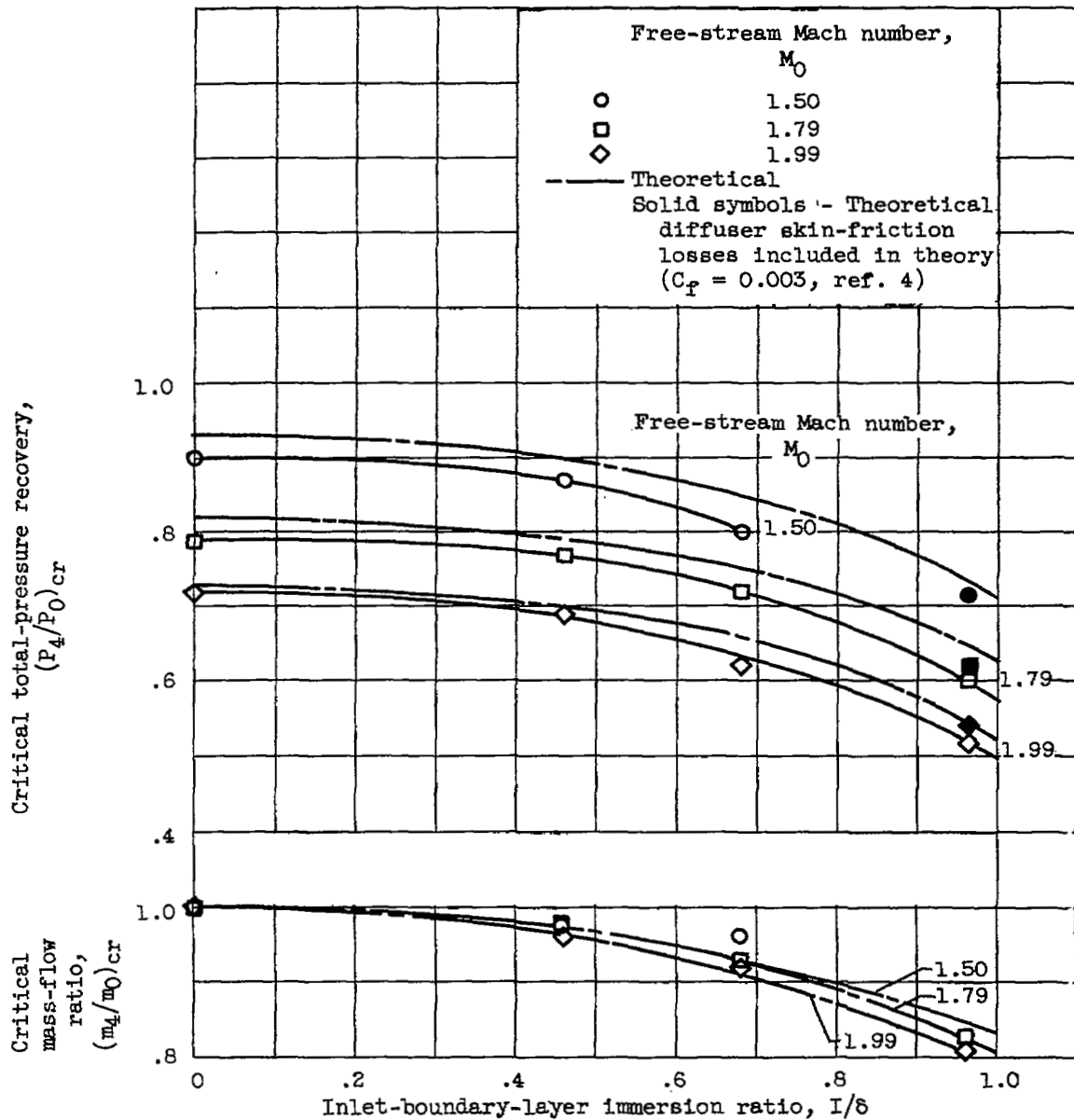


Figure 7. - Continued. Total-pressure recovery.



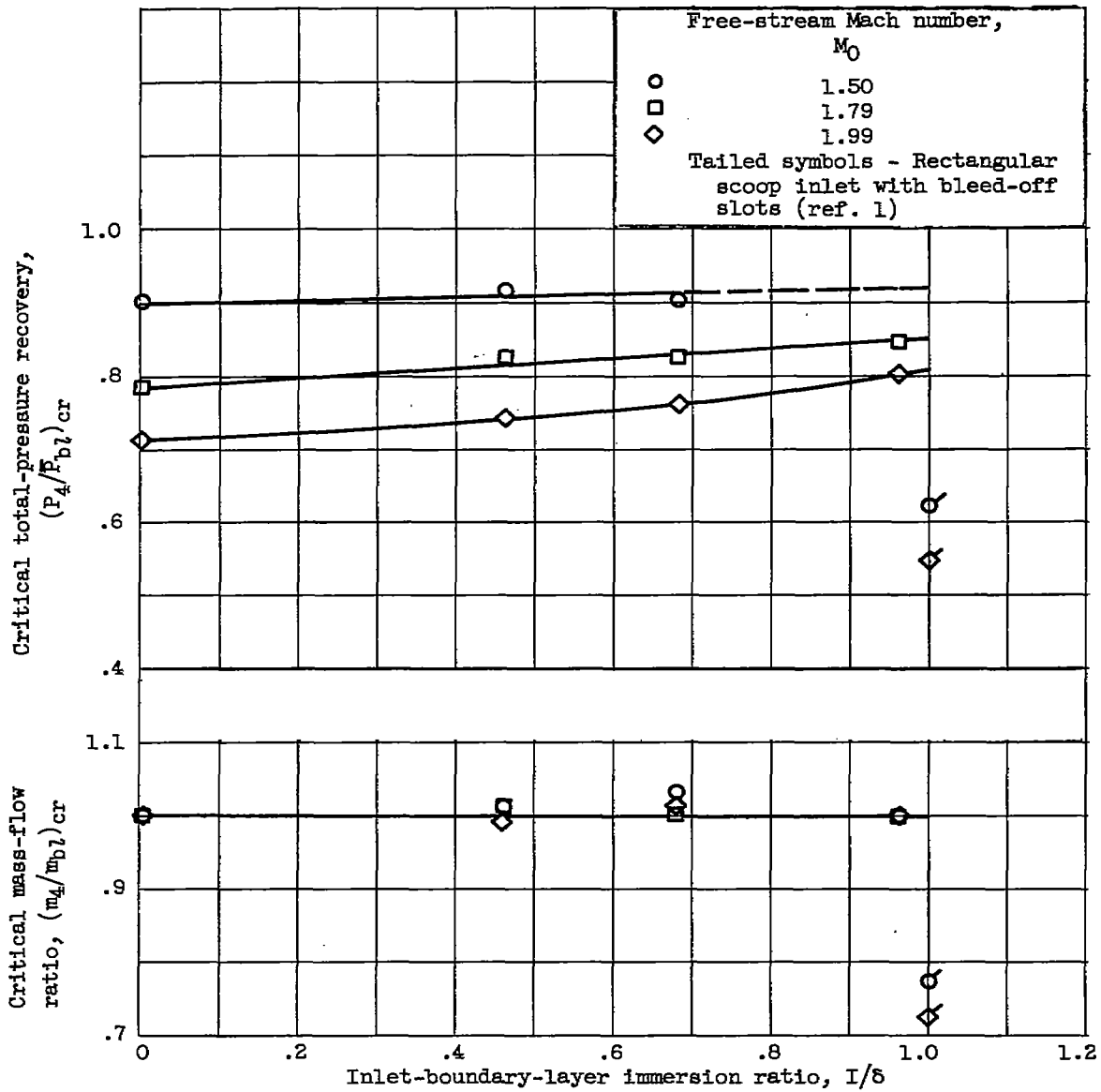
(1) Configuration 4-3.0-3.5.

Figure 7. - Concluded. Inlet total-pressure recovery.



(a) Referenced to free-stream flow.

Figure 8. - Effect of inlet-boundary-layer immersion. Configuration 4-3.0-3.5; top-wall installation.

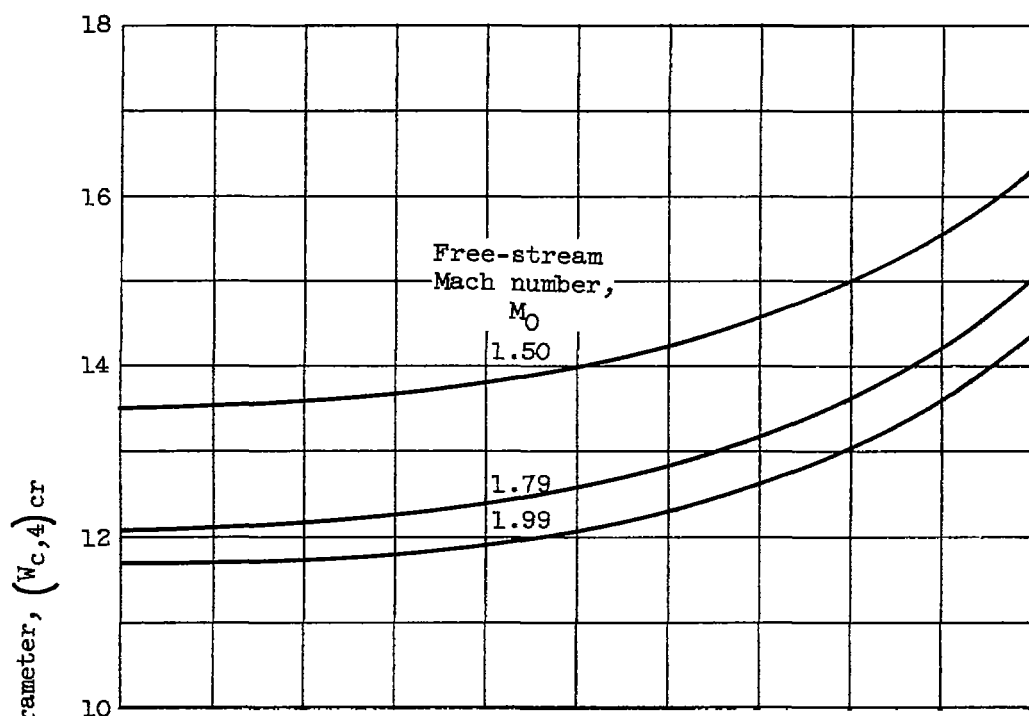


(b) Referenced to boundary-layer flow.

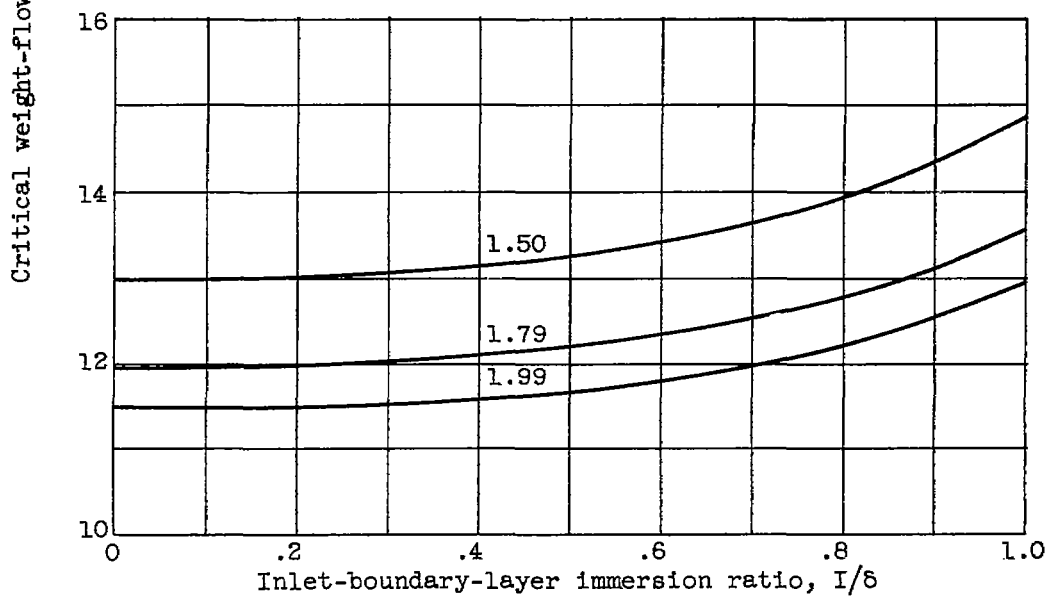
Figure 8. - Concluded. Effect of inlet-boundary-layer immersion. Configuration 4-3.0-3.5; top-wall installation.

5535

UG-4

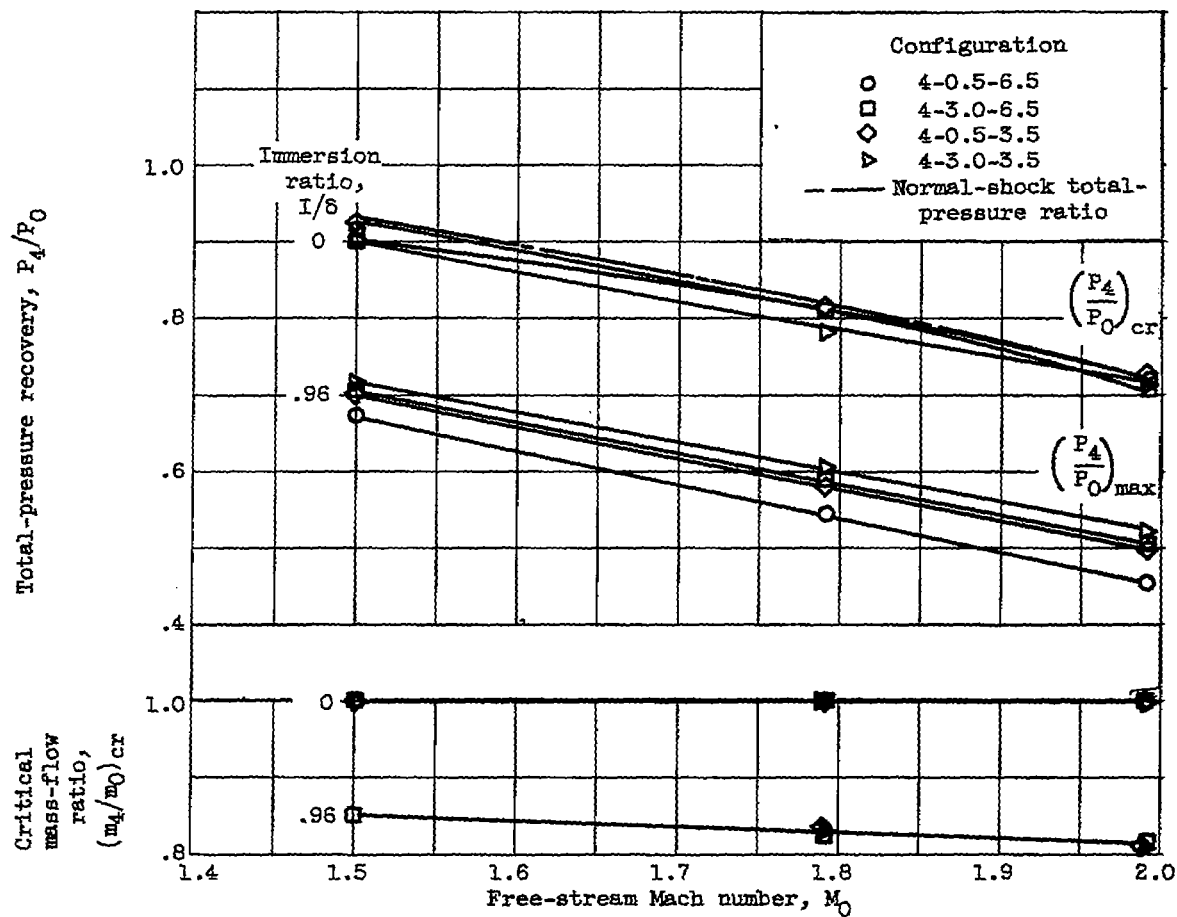


(a) Configuration 2-3.0-3.5.



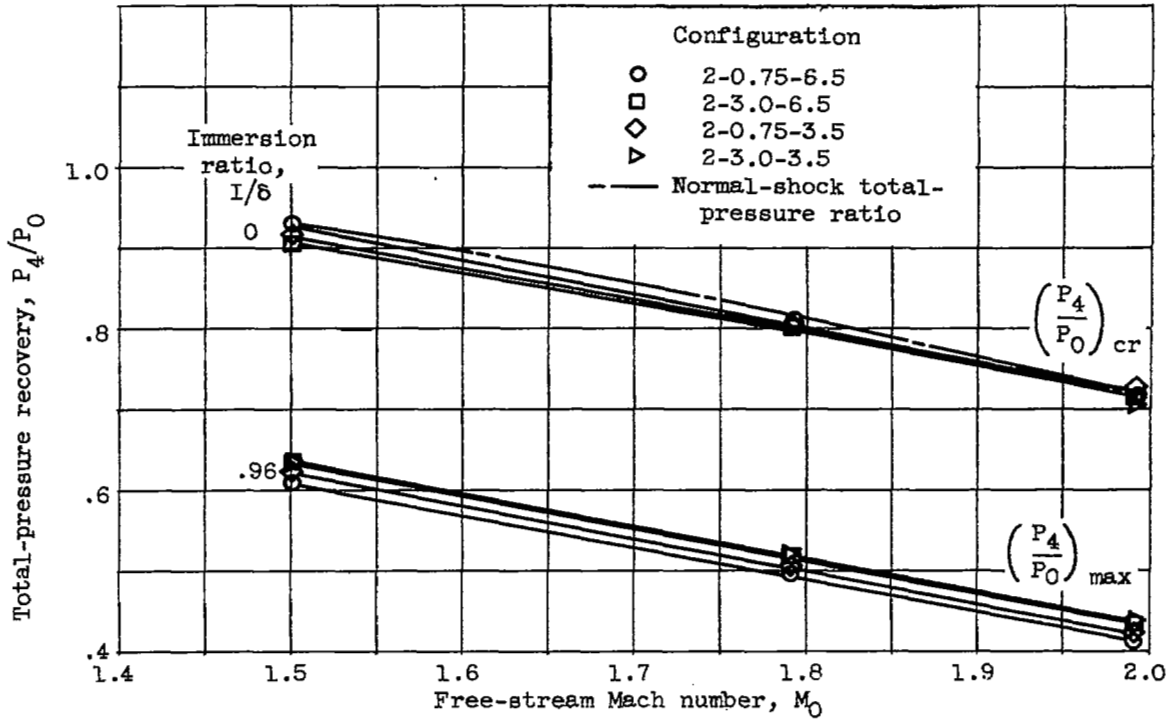
(b) Configuration 4-3.0-3.5.

Figure 9. - Effect of inlet-boundary-layer immersion on critical weight-flow parameter. Top-wall installation.



(a) 4-Inch-diameter inlet.

Figure 10. - Effect of length of inlet constant-area section and diffuser angle. Top-wall installation.



(b) 2-Inch-diameter inlet.

Figure 10. - Concluded. Effect of length of inlet constant-area section and diffuser angle. Top-wall installation.

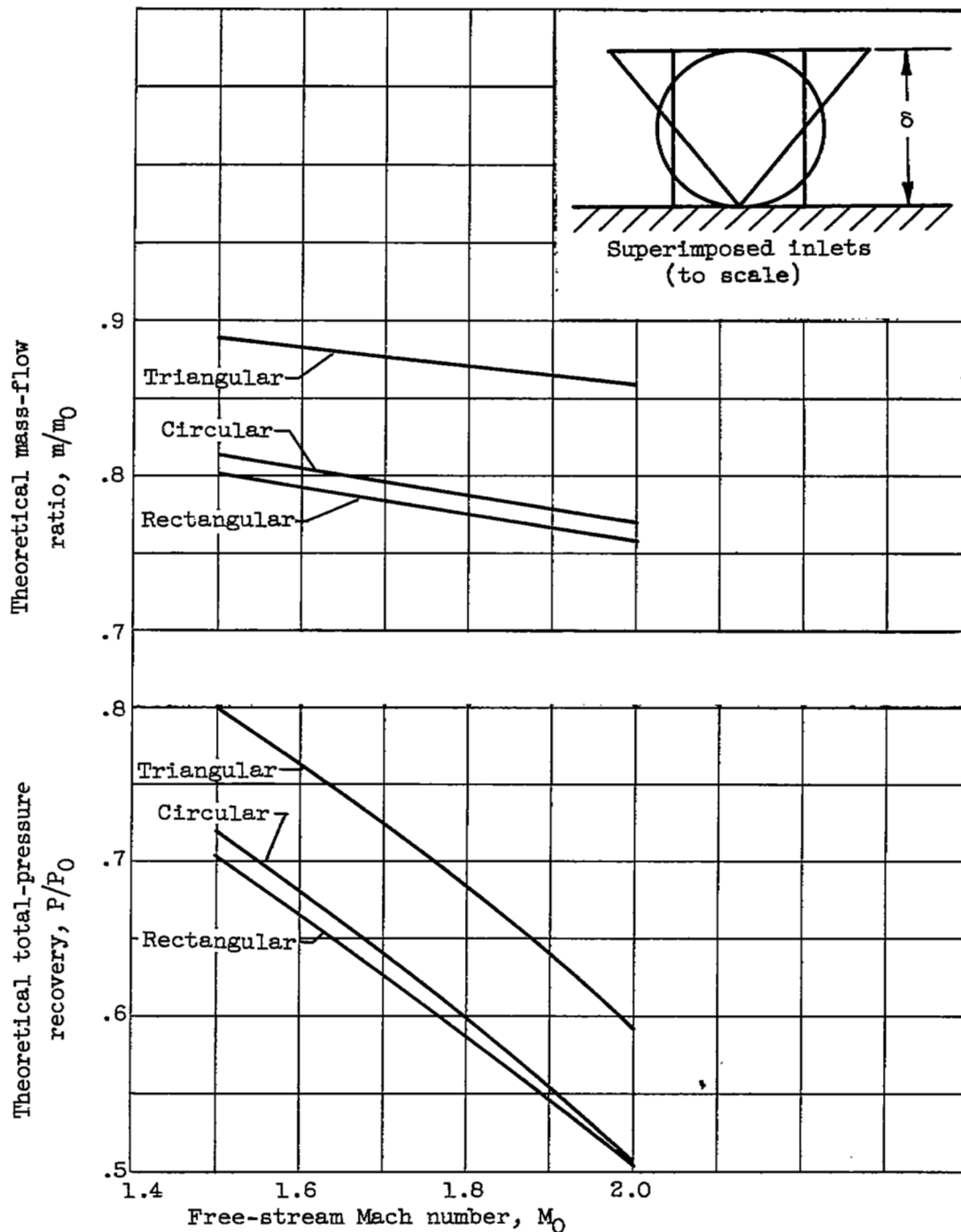
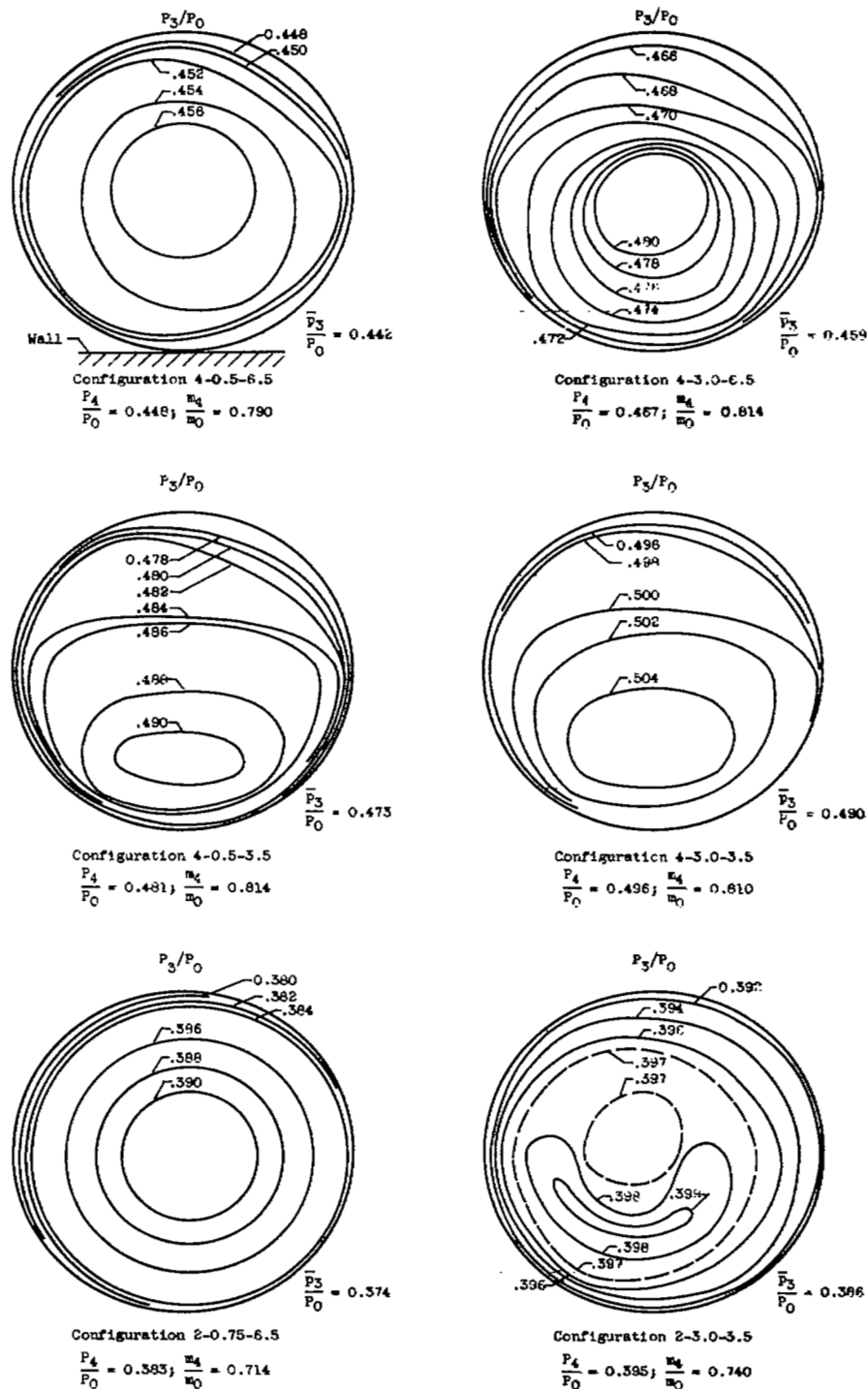
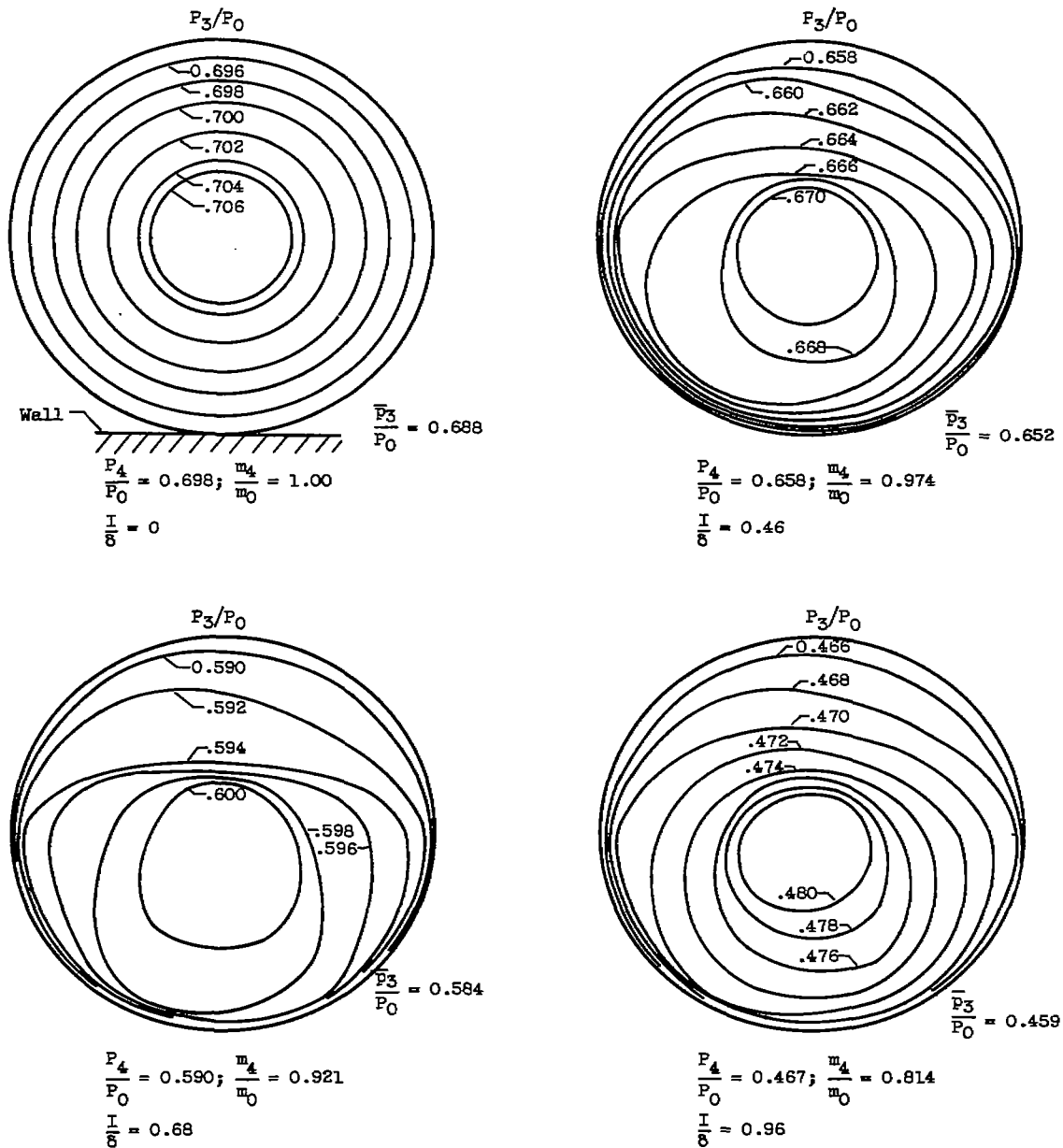


Figure 11. - Theoretical inlet performance of several frontal shapes having equal areas and heights. Inlet-boundary-layer immersion ratio, 1.0; $u/U_0 = (y/\delta)^{1/7}$.



(a) Effect of variations in inlet geometry at critical inlet conditions. Inlet-boundary-layer immersion ratio, 0.96.

Figure 12. - Total-pressure-ratio contours at diffuser exit. Top-wall installation; free-stream Mach number, 1.99; viewed downstream.



(b) Effect of inlet-boundary-layer immersion at critical inlet conditions. Configuration 4-3.0-6.5.

Figure 12. - Concluded. Total-pressure-ratio contours at diffuser exit. Top-wall installation; free-stream Mach number, 1.99; viewed downstream.

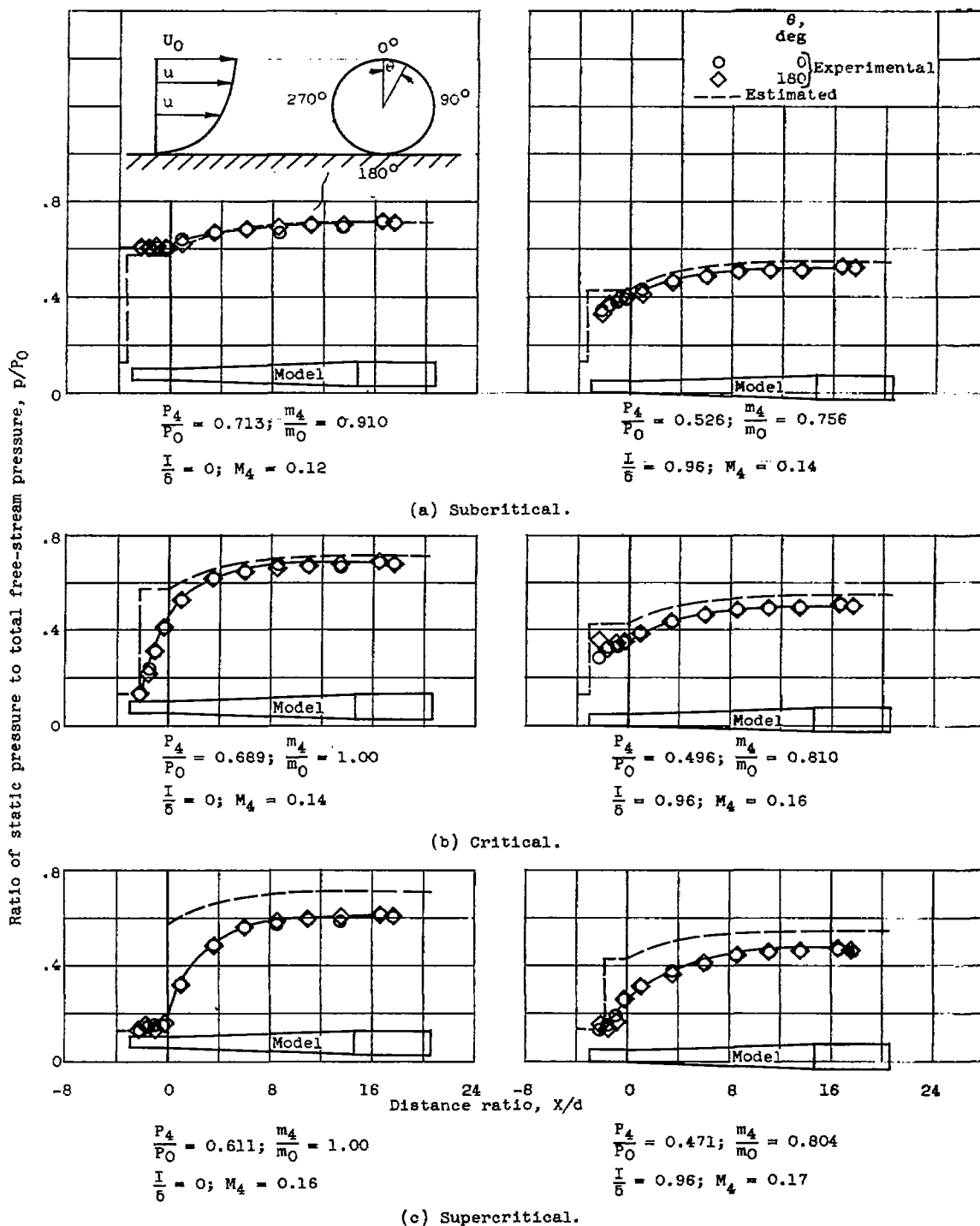
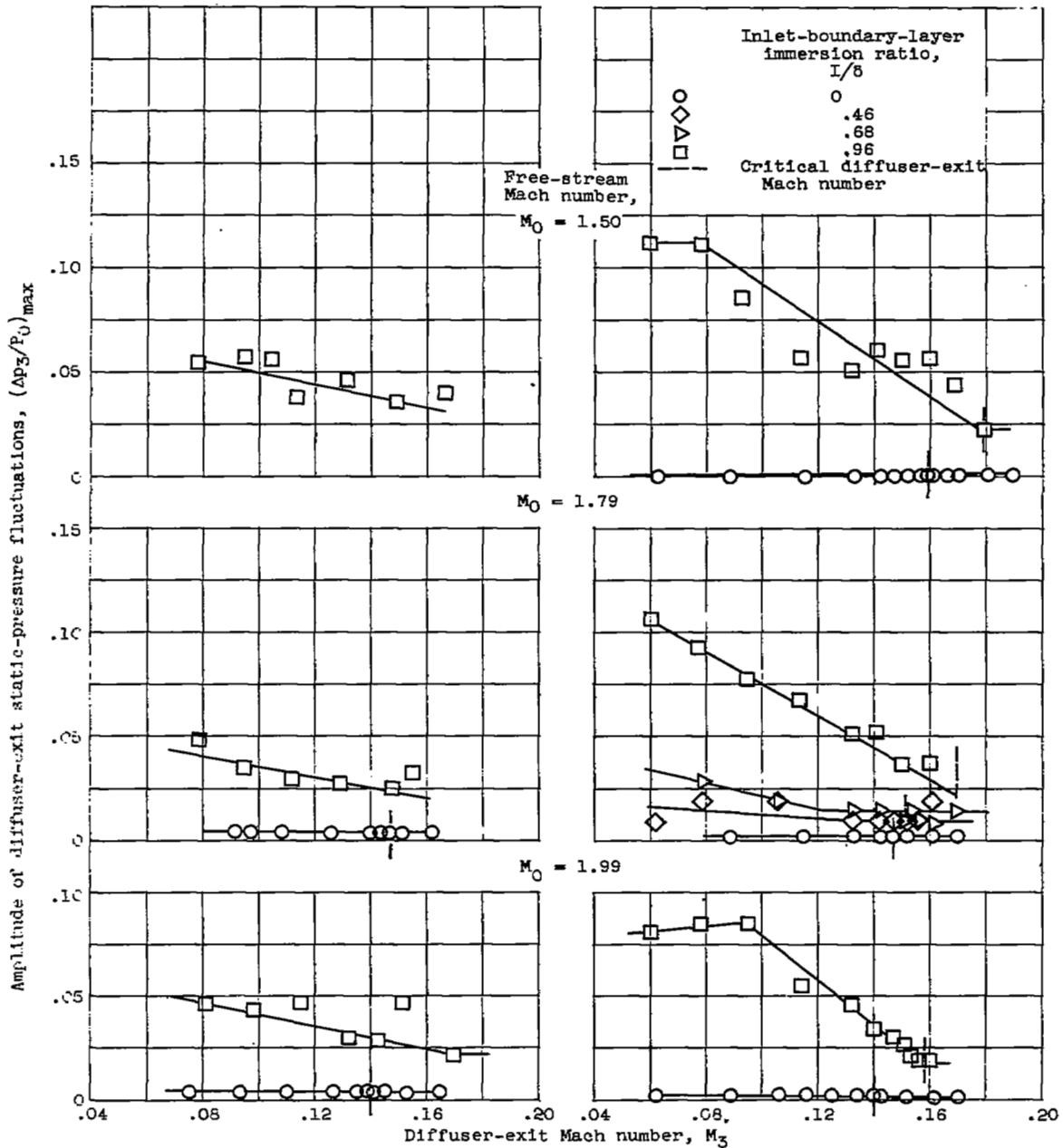


Figure 13. - Diffuser static-pressure distribution. Free-stream Mach number, 1.99; configuration 4-3.0-3.5; top-wall installation.

3535



(a) Configuration 2-3.0-3.5.

(b) Configuration 4-3.0-3.5.

Figure 14. - Diffuser-exit static-pressure fluctuations. Top-wall installation.

[REDACTED]



NASA Technical Library

3 1176 01435 7736

[REDACTED]